Trabajo Fin de Master:
Validation of the mechanical properties of sintered material through the use of microprobes

Student: Nicolas Brunaut,
Tutor: Vicente Amigó Borrás

UNIVERSITAT POLITÈCNICA DE VALÈNCIA

January, 10, 2021

Contents

Acknowledgements

I would first start this acknowledgment by thanks with all my heart my tutor, Vicente Amigo Borras which had taken time to receive me in his laboratory. Through this entire semester he worked with me and was every time able to explain, guide and lead my research. This report and this research would have not existed without him.

He was not the only person to help me for this research, as matter of fact the entire team of the laboratory with their kindness were there to help me. I would like to thank especially Mariana Rossi, doctoral student who has taken in her precious time to explain and stay with me during hours working on the issues I had for my research.

Finally, my last but not least acknowledgement goes for Louise Collot a friend of mine. She was there to help me for the written part of my report, and she enables me to save a lot of time. In addition, her support along the years and especially for this semester was always kind and full of love.

Resumen

En este trabajo, se determinan las propiedades mecánicas de tres tipos de aleación de titanio (titanio puro grado 3, titanio-niobio-estaño y titanio-niobio-circonio-tantalio) a través de dos tipos de ensayo. Estos dos ensayos fueron realizados por dos máquinas diferentes, una máquina de "Small Punch Test" y otra de microtracción presentada al inicio de este informe. Estos dispositivos permitieron determinar el carácter dúctil de la aleación de titanio puro grado 3 y de titanio-niobio-circonio-tantalio. Por el contrario, se establece que la aleación de titanio-niobio-estaño presenta un carácter semifrágil. La aleación titanio puro grado 3 presenta una fase α en su mayoría, mientras que las aleaciones de titanio-niobio-estaño y titanio-niobio-circonio-tantalio muestran mayormente fase β. Los resultados mecánicos obtenidos por las diferentes aleaciones son los siguientes: Pmax = 1207N por el titanio puro grado 3, alrededor de los 260N para el Pmax de los diferentes tipos de aleación de titanio-niobio-estaño y Pmax=1536N por el titanio-niobio-circonio-tantalio. Estos resultados proporcionados por el Small Punch Test se ajustan adecuadamente a los conocimientos estudiados en esta área. No obstante, los resultados extraídos de la microtracción muestran unos órdenes de magnitud por debajo de lo esperado teóricamente.

Aunque los resultados obtenidos no han podido ser totalmente verificados y están a la espera de serlo a través de un estudio numérico u otros estudios físicos, las correlaciones entre los dos ensayos han permitido descubrir un vínculo prácticamente directo entre las energías de fracturas entre probetas de ambos ensayos, con un $R^2 = 0.9694$. Sin embargo, la correlación entre $Pmax$ y σ_{uts} permite tener un $R^2 \geq 0.89$ lo que indica unos vínculos fuertes.

Palabras claves: Small Punch Test/Microtracción/ Titanio puro grado 3/ Titanio-niobio-estaño / Titanio-niobio-circonio-tantalio/Correlación

Resum

En aquest treball, es determinen les propietats mecàniques de tres tipus d'aliatge de titani (titani pur grau 3, titani-niobi-estany i titani-niobi-zirconi-tantalio) mitjançant dos tipus d'assaig. Aquests dos assajos van ser realitzats per dues màquines diferents, una màquina de "Small Punch Test" i una altra de microtracció presentada a l'inici d'aquest informe. Aquests dispositius van permetre determinar el caràcter dúctil de l'aliatge de titani pur grau 3 i de titani-niobi-zirconi-tantali. Per contra, s'estableix que l'aliatge de titani-niobi-estany presenta un caràcter semifràgil. L'aliatge titani pur grau 3 presenta una fase α en la seua majoria, mentre que els aliatges de titani-niobi-estany i titani-niobi-zirconi-tantali mostren majorment fase β. Els resultats mecànics obtinguts pels diferents aliatges són els següents: Pmax =1207N pel titani pur grau 3, al voltant dels 260N per el Pmax de als diferents tipus d'aliatge de titani-niobi-estany i Pmax = 1536N el titani-niobi-zirconi-tantali. Aquests resultats proporcionats pel Small Punch Test s'ajusten adequadament als coneixements estudiats en aquesta àrea. No obstant això, els resultats extrets de la microtracció mostren uns ordres de magnitud per davall de l'esperat teòricament. Encara que els resultats obtinguts no han pogut ser totalment verificats i estan a l'espera de ser-ho a través d'un estudi numèric o altres estudis físics, les correlacions entre els dos assajos han permés descobrir un vincle pràcticament directe entre les energies de fractures entre provetes dels dos assajos, amb un R^2= 0.9694. No obstant això, la correlació entre $Pmax$ i σ_{uts} permet tindre un $R^2 \geq 0.89$, el que indica uns vincles forts.

Paraules claus: Small Punch Test/Microtracció/ Titanio pur grau 3/ Titanio-niobio-estaño / Titanio-niobio-circonio-tantalio/Correlació

Abstract

In this work, mechanical properties of three types of titanium alloys (commercial pure grade 3 titanium, titanium – niobium- tin and titanium-niobium-zirconium-tantalum) have been determined through two types of test. These two tests made by a Small Punch Test device and the device of microtension explained at the beginning of this report enables to determine the ductile behaviour of the commercial pure grade 3 titanium, titanium and titanium-niobium-zirconium-tantalum on the contrary of the alloy titanium – niobium- tin which is semi brittle. The alloys made by α phase in majority for the commercial pure grade 3 titanium and by β phase in majority for the titanium – niobium- tin and titanium-niobium-zirconium-tantalum have obtained coherent results with the actual knowledge of this area (Pmax=1270N for the commercial pure grade 3 titanium, Pmax value near the 260N for the different types of titanium – niobium- tin alloys and 1536N as Pmax value for the titanium-niobium-zirconium-tantalum). Nevertheless, results from the microtension test are lower by several orders of magnitude in comparison with the actual literature.

Even if the results obtained needs to be reevaluated through a numerical test or a new physical test, correlation between the two tests have enabled to find out a strong link between the energy of fracture of the two tests with a R^2=0.964. However, the correlation between $Pmax$ and σ_{uts} found an $R^2 \geq 0.89$ which shows a strong link.

Key words: Small Punch Test/Microtension Test/ commercial pure grade 3 titanium/ titanium – niobium- tin / titanium-niobium-zirconium-tantalum/Correlation

List of Figures

List of Tables

1 Introduction

1.1 State of the art of Small Punch Test

1.1.1 History

The evaluation of the mechanical properties has always been an active field of study along the last centuries. However, despite the fact that there is a lot of different technique, it exists only few methods to determine the mechanical properties in a non-destructive way (CHERFAOUI, 2006; Vautrot, n.d.) . In addition, these techniques are not the famous ones and there are fewer documents, papers on these non-destructive characterisation technique.

Here comes the Small Punch Test (**SPT**) (also call: *Miniaturised Disc Bend Test*) . It is a technique which is situated at the border of the non-destructive and destructive characterisation technique. Indeed, the SPT is a test where only a few quantity of material is used and destroyed or affected by a non-reversible mechanical action. However, the quantity used during the test is so small that some authors call it like a non-destructive technique (Janca et al., 2016; national Members, 2007; Wen et al., 2016).

This method has been well developed, first, for the determination of properties in nuclear power station. Indeed, as the material could be radioactive and then consequently dangerous for the operator, it was mandatory to analyse small material of it, as the radioactivity is directly dependent of the size of the material. The investigation was started first in the eighties by Manahan, 1983 at the MIT and then in the nineties by MAO and TAKAHASHI, 1987. Theses two articles are the prequel of other researches which are still a current field of study (García et al., 2013; Simonovski et al., 2020; Simonovski et al., 2016; Wen et al., 2016) .

1.1.2 The Small Punch Test technique

In this section, the Small Punch Test technique will be described and defined. It will also be explained how to analyse the curve of a SPT, the data that can be extracted from this curve and how to extract the data properly from this curve. Finally, a presentation on how to correlate the data from a SPT with data normal/bulk size test. After presenting the different correlation, a discussion on their usefulisation and accuracy will be done.

i Definition

In order to understand the test, it is important to start with a definition of the technique. The SPT can be defined as the following words: *It is a deflection of an embedded from its outside part disk. The deflection occurs in its central part through a compression due to a ball or a round head rod. This process can be led until the fatigue and rupture of the material. This process is able to give the mechanical behaviour of the material tested* (Avila, 2019). It can be assimilated at the biaxial test used in ceramics very well studied for the dentistry (Albakry et al., 2003; Morrell, Review in 2007).

ii Device and sample

The device

Figure 1 and figure 2 show the set up of the sample. The first image enables to see the overview of the set up done by Solidworks in order to fabricate it, while the second one is the set up with a section view. In the majority of the case the experimental device as a circular hole in its base of diameter Dp. This rigid base is exempt of straight angle in order to avoid an accumulation of the deformation during the compression. It is on this base that the sample is put, and is embedded by the upper part as shown in figure 2. The upper part will be set on the sample thanks to screw in order to embedded it well. This part also has a hole (Ds as diameter), in order to let the rod cross it and to push the ball previously put on it.

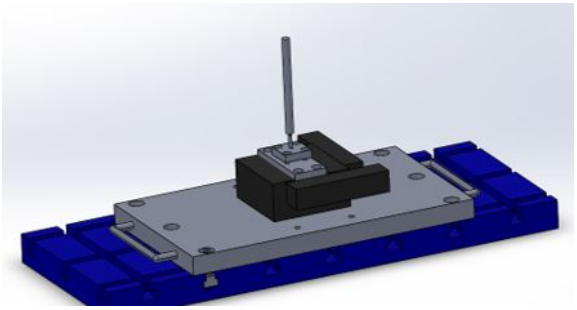

Figure 1: Small Punch Test Machine overview with Solidworks

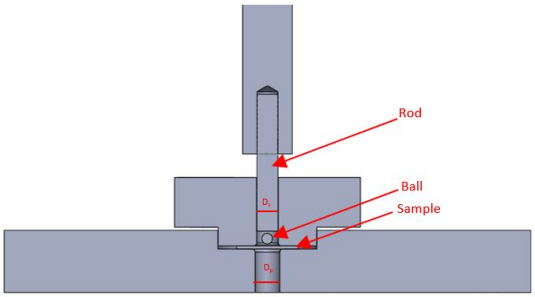

Figure 2: Small Punch Test Machine focus on the rod. Ds: Diameter of the hole in order to let the rod pass and Dp: diameter of the hole

All of this set up is put in an universal testing machine. This enables to get directly the data of the displacement of the rod, and the force which is applied on it through the software used by the mechanical testing machine.

The European Committee for Normalisation (**CEN**) preconceived to work at room temperature, at the normal atmosphere pressure with constant velocity. The Dp diameter must be of 4.35 mm (national Members, 2007).

The sample

The sample is used to be a circular disk of 0.5mm of thickness by 8 mm diameter (García et al., 2013; Janca et al., 2016; Simonovski et al., 2016). Even if the first investigation were done with 3 mm diameter (Manahan, 1983; MAO and TAKAHASHI, 1987). The material needs to be grinded by a P1200 in order to avoid straight angle and consequently a concentration of the force during the test (national Members, 2007). This grinding has a second usefulity, it enables to reach the thickness required after the cutting process.

It is really important to manage to have a thickness almost constant or with relatively small variation because it can change the value of the SPT curve significantly. In addition, having a constant thickness among the probe enables to have an homogenous surface However, not only the thickness is directly linked to the results, but the diameter of the ball and the diameter of the hole of base too.

The dimension of the probe, the diameter of the ball, and from the hole of the base have been studied. An augmentation of the thickness, with constant other value cause an augmentation of the value of the maximal force. If the diameter of the ball increase, while the two other values stay constant, makes the inflexion point increase. Finally, if the diameter of the hole of the base decrease, while the two other values are fixed, the maximum force increase (Avila, 2019).

iii Deformation during the Small Punch Test

During the test, the force and the displacement of the rod are continuously register. This enables to have the famous Force-Displacement curve of the sample as shown in figure 3. The force-displacement curve is well known to be able to give the mechanical behaviour of the materials. This one is not exactly the same as the tension test curve. However the deformation is quite similar and has a lot in common as the tension test curve.

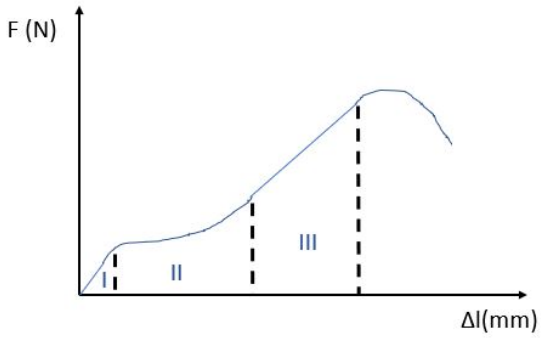

Figure 3: Typical curve of a Small Punch Test

As shown in the previous figure, the curve can be divided in 4 regions.

- The first one, represented by I, is the initial indentation where the centre of the probe is in the elastoplatic zone, and where, the rest of the probe is in the elastic zone.
- The second one, represented by II, is where start the process of plastification of the centre of the probe and around it.
- The third one, represented by III, is the traction and stretching of the membrane. It is where the plastification follow a linear curve.
- The last part is when the probe has reached the failure, the maximum of the plastic deformation is reached and the rupture is done.

iv Determination of the mechanical properties

In this part, the presentation of the determination of the mechanical properties will be done.

This part will focus on the determination of the P_y value through only few techniques, the more common that are described by Janca et al., 2016, and then the energy and the plastic instability studied by Avila, 2019. After this focus, the other mechanical properties will be explained and a demonstration on how to extract them will be done.

The different technique to get the P_y value has been developed along the decades first by MAO and TAKAHASHI, 1987 and then by other authors in order to be more accurate, and find better correlation with the tension test curve data.

Obviously, nowadays the CEN has normalised the determination in order to have the same way to get the results and then compare them (national Members, 2007).

From, the figure 4, the famous force-displacement curve, it is possible to extract different type of value as said previously, such as the following:

- P_y: The force (in newton) that represents the yield stress. It can also be called the F_E.
- P_m: The maximal force (in newton) that the sample can hold
- Z_m: The displacement (in millimetres) where the force is the maximum
- E_{SPT}: The energy (in $MPa * m^{0.5}$) until the fracture, the area under the curve
- The plastic instability given by the intersection of the curve and the dF/dz curve

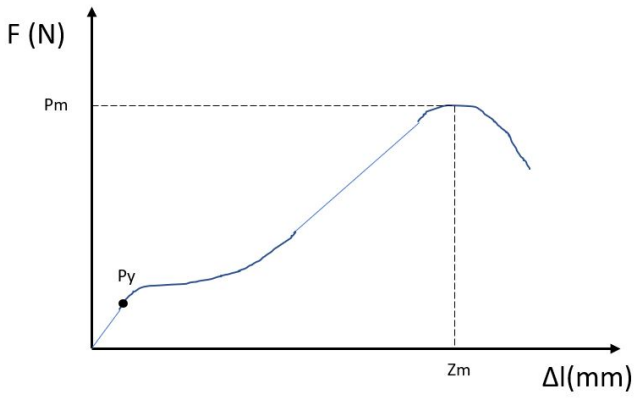

Figure 4: Different types of value available in the SPT curve

The P_y value

It is very important, in a study to indicate the way to determinate the P_y, as it is shown in the figure 5, the different values of the P_y are not all the same and can be quite different regarding the material.

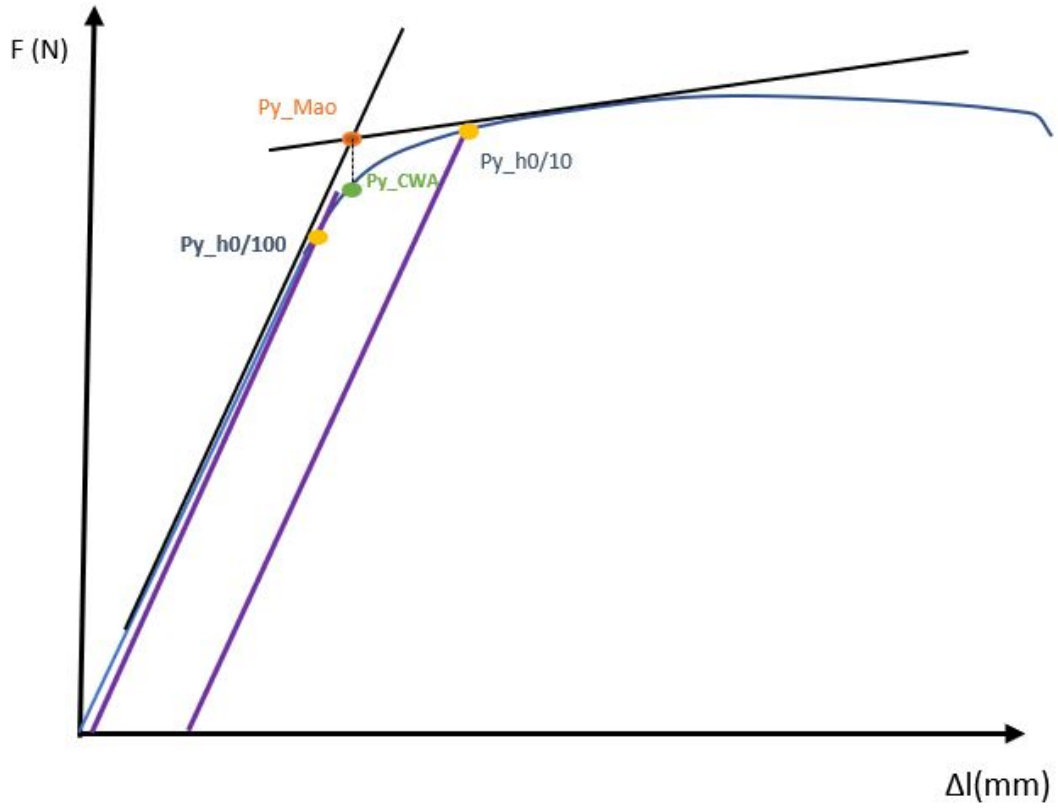

Figure 5: Determination of the mechanical properties in the SPT curve

In figure 5, it is possible to see different types of determination of P_y.

- Py_{MAO}: It is the technique determine by MAO and TAKAHASHI, 1987. This value is the intersection of the two tangents in the elastic and plastic zone.
- Py_{CWA}: This value is the value recommended by the CEN, it is the intersection between the SPT curve and the vertical line from the Py_{MAO} value.
- $Py_{ho/10}$: This value it set at the intersection between the line defined by the parallel of the elastic zone, and with the point: $(h_{0/10}; 0)$ and the STP curve. Where h_0 is the initial thickness.
- $Py_{ho/100}$: This value it set at the intersection between the line defined by the parallel of the elastic zone, and with the point: $(h_{0/100}; 0)$ and the STP curve. Where h_0 is the initial thickness.

As said previously, the CEN has normalised this determination, with the Py_{CWA} value. However, in some cases, the determination of the tangents in order to get the Py_{MAO} and then the CEN value, is not always easy, especially with brittle or semi-brittle materials, that is why in some cases, the other techniques are used. Indeed, in brittle or semi-brittle materials, as the plastic zone is not obvious or non-existing, it is impossible to have a tangent from this part and then the intersection with the other one.

The energy

It is also possible to get the energy of the fracture, thanks to the integration of the curve (the area above the curve).

The energy can be defined until the finale of the curve or until the maximum of the force. The energy is given by the equation 1

$$E_{SPT} = \int_0^{Z_m} \left\| \overrightarrow{F(z)} \right\| dz \tag{1}$$

Obtaining the energy value can lead to the fracture toughness of the material and consequently gain time and material in order to avoid doing a Charpy Test.

The plastic instability

During a test, or utilisation the deformation of a piece due to stress occurs in the weakest region, that could be the smaller area, or the area which is damaged. During the lower strains there is a uniform deformation due to the fact that the weakest section is the least deformed section. When the strains become higher the most deformed region is the weakest, this lead to a concentration of the deformation and consequently forming a neck (Hosford and Caddell, 2011). After the formation of the neck reached, it occurs the plastic instability.

Plastic instability is defined as *the growth of a locally thinned region or neck in a material upon the application of stresses* (Duncombe, 1972). In other world, it is the time where the hardening in the neck is not enough to overcome the stress provoked by the tensile test. After reaching this point, the deformation increase faster than before.

In a mathematical point of view it can be seen as the equation 2. Indeed, as the hardening is no longer true, after this point, there is a drop of the differentiate curve, and the plastic instability is defined as the intersection with the curve as it is shown in the figure 6.

$$d\sigma/d\epsilon = \sigma \tag{2}$$

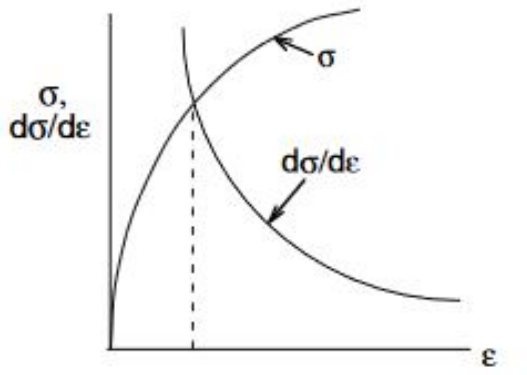

Figure 6: Determination of the plastic instability in a stress-strain curve (Hosford and Caddell, 2011)

This intersection is able to give us the value of σ_{uts} and ϵ_u, which are respectively the maximum load in tension, and the maximum uniform deformation (Avila, 2019; Hosford and Caddell, 2011).

In a SPT-curve, as the representation is the force depending of the displacement, the analogy can be done. The differentiation is not done on the stress but on the force as the equation 3 and the figure 7 show it.

$$dF/dz = F \tag{3}$$

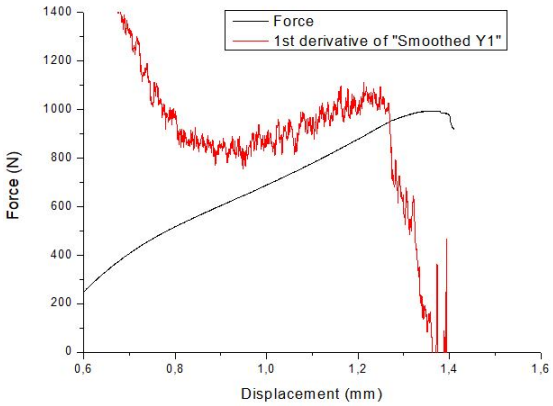

Figure 7: Determination of the plastic instability in a force-displacement curve of the CPTi-1 probe

This intersection is able to give us the value of P_c and z_c, which are respectively the maximum force in tension, and the maximum uniform displacement (Avila, 2019).

v Correlation between Small Punch Test and conventional test

Correlation between the Small Punch Test and conventional test as for example microtension test or tension test have been studied along the years, and are still a current field of investigation (García et al., 2013; Janca et al., 2016; MAO and TAKAHASHI, 1987; Simonovski et al., 2020). Indeed, even if a force-displacement curve is able to give a good global idea of the mechanical behaviour of a material (brittle, semi-brittle or ductile) or a good comparison between different materials, this is not enough and it is more common in the literature to extract from this kind of test the information for metallic materials such as the maximum stress, maximum deformation, the yield stress and Young's modulus.

As, in this report, the main work is focus on the correlation with the microtension test, this part will focus on the correlation with it. However, it is possible and there is a huge lack of information on other correlation with other types of test such as the Charpy test in order to reach the fracture toughness value.

MAO and TAKAHASHI, 1987 proposed a simple empirical and linear relation to correlate the load P_y and the yield stress σ_y for *both 3 mm X 0.25 mm TEM disk and 10 mm square X 0.3-0.5 mm specimens*. The correlation can be expressed by the equation 4, where t_0 is the initial thickness of the SPT probe.

$$\sigma_y = 360 P_y / t_0^2 \tag{4}$$

In the same article, they propose to correlate the load maximum P_{max} and the ultimate tensile stress σ_{uts}. They have found that for *3 mm X 0.25 mm TEM disk and 10 mm square X 0.5 mm specimen*, the empirical correlation between them can be expressed as the equation 5 where t_0 is the initial thickness of the SPT probe.

$$\sigma_{uts} = 130 P_{max} / t_0^2 - 320 \tag{5}$$

The equation 4 and 5 have been developed at the beginning for all metallic materials. However, nowadays with the increase of results given by different laboratories it has been shown that theses two equations are not totally accurate, and especially because disk of 5 mm of diameter by 0.5 mm of diameter are mostly used to do SPT. In addition, these correlations have been done on a huge number of different materials, and this relation is not applicable for a specific one nor specific technique use to proceed the probes. Due to that general equation has been developed and used over the years. The yield ultimate strength (σ_{ys}) have been correlated through a linear equation, (equation 6) depends of the initial thickness elevated at the order 2. This correlation is well accepted by the literature for the entire range of materials tested by the SPT. All factors α_1 and α_2 are factors given by the empirical linear relation and they are dependant of the material.

$$\sigma_{ys} = \alpha_1 P_y / t_0^2 + \alpha_2 \tag{6}$$

Nonetheless, some correlations between the ultimate tensile strength σ_{uts} and the maximum of the force P_m have been developed as seen with the equation 7, equation 8 and equation 9.

Indeed, the majority of authors are using the equation 7 which seems the more accurate correlation (Avila, 2019). Notwithstanding, according some authors the P_m value is depending of the thickness at the order one (García et al., 2013) and not by the thickness at the order 2. A last correlation given by the equation 9 correlate the ultimate tensile strength with the thickness multiplied by the value of the displacement while the force is at its maximum (z_m). All factors $\beta_1, \beta_2, \beta_1', \beta_2', \beta_1''$ and β_2'' are factors given by the empirical linear relation. They are dependant of the material.

$$\sigma_{uts} = \beta_1 P_{max} / t_0^2 + \beta_2 \tag{7}$$

$$\sigma_{uts} = \beta_1' P_{max} / t_0 + \beta_2' \tag{8}$$

$$\sigma_{uts} = \beta_1'' P_{max} / (t_0 * z_m) + \beta_2'' \tag{9}$$

In 2018, Jose Calaf Chica, 2018 have found a new correlation between the initial Slope call $Slope^{inti}$ and the yield strength. The initial slope is the slope given in the part one of the typical SPT curve (see figure 3). This correlation, contrary to the previous one, is an exponential relation given by the equation 10. The factor a and b are the correlation factors which are obtained from regression analysis.

$$\sigma_{uts} = a * e^{b * Slope_{initi} / t_0} \tag{10}$$

As shown in figure 8, the correlated factor is $R^2 = 0.996$, which shows a strong correlation.

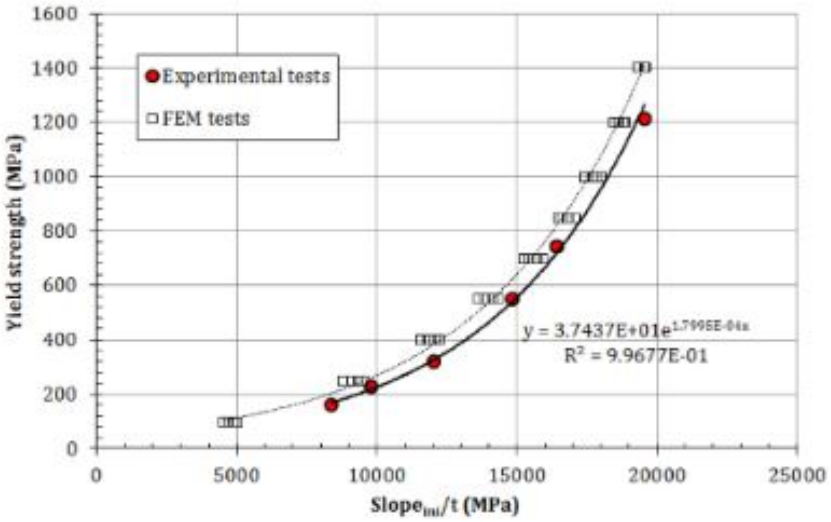

Figure 8: Correlation between the $Slope^{inti}$ and the yield strength Jose Calaf Chica, 2018

1.1.3 Advantages of the Small Punch Test

The Small Punch Test as also huge number of advantages. As said previously, it is an important gain of material. As for example, with a metallic bar of 100 mm of length, it is possible to get 3 normal size traction probes, and 70 small size probes (Avila, 2019). Consequently, there is more probes, so it is easier to get more accurate means, and shorter result's deviation due to the important number of probes that it is possible to get through one sample.

Another important point, that could be noticed is the gain of time and money. Since there is a reduction of the quantity of material, there is obviously a diminution of the cost by using a small quantity of material.

The no so obvious other advantage is the gain of time. Indeed, as the material is shorter, the time to deform it will be shorter than a normal size probe, and then consequently it is possible to analyse more probes in the same range of time than with normal size test. As it is possible to get more probes, the means results will be more accurate and less scattered.

It could also be interesting to notice that the SPT is a technique which has the potential to estimate the creep behaviour in high-temperature service (Wen et al., 2016; Yang and Wang, 2003). This technique is also well used in order to analyse small regions of structural components that are impossible with machine normal size probes, such as the heat affected zones of welded joints or thin coatings (García et al., 2013).

This technique, due to the data that are obtained (see part 1.1.2) is a good technique in order to compare rapidly the mechanical behaviour of two different materials or different alloys.

1.1.4 Disadvantages of the Small Punch Test

As all the test, this one is not a perfect test, it as some failures and some difficulties to realise it. Firstly, in order to have the probes, which are less than the millimetre of size, in it's mandatory to have machine able to deal with it, as for example a really good precision slicer and a compress, traction machine able to change its set up for this kind of test.

In addition, this kind of test needs to be normalised. The CEN, has in 2006 done the normalisation for Small Punch Test Method for Metallic Materials (national Members, 2007).

In this Workshop Agreement, there is all the normalise information on the machine of testing itself until the probes itself. With the CEN technique, they used a rod without a ball between it and the sample. It is important to notice that some authors, and actually a majority use a ball at the end of the road as it is possible to see in figure 2. (Avila, 2019; García et al., 2013; Janca et al., 2016; MAO and TAKAHASHI, 1987).

1.2 State of the art of the Microtension Test

1.2.1 History

As it is well known, the size of a piece is directly dependent on the mechanical behaviour of this piece. This, for all kinds of material. The brittle materials or semi-brittle materials are dependent of the *Weibull distribution*, while the crystalline metals are subject to the famous *Hall-Petch Effect* and *Inverse Hall-Petch Effect* (Al-Rub, 2007; George Z. Voyiadjis, 2019). However, the bulk test is well developed and well-known while the small size test (range of nm or mm) is not, which create the problem to characterise new range of objects (microelectromechanical systems, microfluidic devices, nanotechnology), material and consequently use them in good condition, environment (Gudlavalleti, 2002). Indeed, many industrial and searchers agree on the fact *"If you cannot measure it accurately, you cannot construct it"* (TODUA, 2005).

In order to study the comportment of the small size object, different types of experiment have been developed as the SPT as said previously in order to investigates the degradation of irradiate materials, and the Mechanical Testing at the Small Scale call in this report as **Microtension test** (Al-Rub, 2007). Bulk size tension test gives us an idea of the general behaviour of the material while microtension test enables to determine the mechanical properties of small part of the bulk and consequently of a region (different phases, or heterogeneity zone of the sample). The fact that it is possible to determine the properties of only a region on a sample is interesting in different fields such as in bio-mechanical. Indeed in some biomaterials such as the wood, the orientation of the fibre is directly linked to the mechanical behaviour, consequently it is important to use nano-scale or micro-scale sample to determine the properties in the different orientation of the wood (Éric Badel, 1999). It can also be used in 3D printing with polymers or metals. As for the wood, the orientation of the layer given by the printer is linked to the mechanical behaviour (Avila, 2019).

Microtension test involves five subsystems: the specimen, the fixturing system to hold the

specimen, the actuation system to apply a prescribed load or displacement history, the load cell to measure the force being carried by the specimen, and the system to measure the specimen deformation.

1.2.2 The sample

The fabrication of the sample is a critical aspect of the microtension test. Indeed, it is mandatory to keep undamaged the sample after its creation. It is important to take into account the boundaries conditions for the dimension and the shape of the sample. The sample must fit with the fixturing system which holds the specimen.

1.2.3 The fixturing system

The system as a bulk size system has two cross heads in order to fix the system. They must be coaxial with the sample and with the rest of the machine in order to insure a full uni-axial traction. The deformation of the fixturing system itself must be minimised in order to not interfere in the determination of the probability. Different types of grips can be used depending of the behaviour of the sample (Gudlavalleti, 2002). There are 2 main ways to fix the specimen on the grip. The first one by gluing the specimen to the grip (mainly used for thin film), the second one by clamping it (for foil tensile specimen for example). Theses methods are obviously giving different results due to the fact that the stress is not applied equally in both systems.

1.2.4 The actuation system

The actuation system is the system which transmits the force and displacement to the fixturing system and consequently to the sample. Actuation system of small size test must be compact and with the higher accuracy possible. There are different types of actuators such as electromagnetic force coils, motor driven screws and various piezoelectric crystal (Gudlavalleti, 2002).

1.2.5 The load cell

The load cell is, as the bulk system, used in order to determine the load applied on the sample at any time. It is usually an elastic element put in series with the sample, and its strain is related to the strain of the sample with a shift. It is more common to have a stiffer load cell than the sample in order to have a non-excessive load on the load cell itself.

1.2.6 Deformation measurement

This is the system which measures the deformation or strain of the sample. It works as the same as for the bulk system. However it must be more accurate, and more frequent to measure the deformation. It exists different way to obtain it. First, with the displacement of the cross head. However, in order to respect the premise of *Saint-Venant*, it is important to measure the deformation in the valuable area of the sample. In order to do it in a proper way, some contact and non-contact

extensometer have been developed. The advantage of a non-contact extensometer is the non-interaction with the sample during the deformation, the rigidity, friction of the extensometer itself. That is why, optical extensometers have been developed.

1.2.7 Survey of existing machine

This section will summarise three different types of existing micro-tensile machine in order to give an idea of this type of machine that can exist. However, these three are not the only three one that exists, and it is also interesting to note that some bulk size machines have been adapted with some modification to micro-size tensile test.

The three machines are the following one:

- The microsample tensile tester at Johns Hopkins University developed by W. N. Sharpe and Edwards., 1997.
- The NIST microtension testing machine developed by Read., 1998.
- The microtension testing machine at Harvard University developed by J. Ruud and Spaepen., 1992.

i The microsample tensile tester at Johns Hopkins University

The actuation system works with a motorised dovetail slide system, this system uses different commercial grips. The actuation system is fabricated to rotate a lead screw which generates a translation rates from $2\mu m/s$ to $20\mu m/s$. To overcome friction, the end of the grip is carried by a linear air bearing. The other grip is directly linked to the cell load.

Base on the sample and its mechanical behaviour, it can be fixed on the grip with glue or inserting a screw in its middle of its head.

The measurement of the strain can be done with an optical method which increase the accuracy of its measurement.

ii The NIST microtension testing machine

The actuation system of this machine is led by two 60 mm long piezoelectric stacks. The sample is set between two grips, a first one which is fixed and a moving for the second one. The moving grip is supported by a load sensing cantilever beams. In order to measure the displacement, a non-contact technique is used through an eddy current displacement system.

In order to use this system properly, it is recommended to use it in small displacement, otherwise the cantilever load system will affect the coaxiality of the all machine.

iii The microtension testing machine at Harvard University

The actuation system of this machine is a motor or piezoelectric system. This machine is the most common one. The main advantage of this machine is the determination of the strain. The

deformation is measured by an optical way. However, in a majority of cases, there are only two dots to measure the displacement. Here, there are four points set as a rectangle in order to determine the longitudinal and transverse displacement.

1.3 Motivation

Alloys of titanium are nowadays used in many fields manly due to its great chemical properties in corrosion, fire-resistant, bio-compatibility but also for its mechanical properties.

In the aim of developing new alloy base on titanium for biocompatible prosthesis the metallurgic powder department of the Polytechnic University of Valencia have created and working on 2 different titanium-based alloy (Titanium-Niobium-Tin and Titanium-Niobium-Zirconium-Tantalum).

As said previously, the two alloys of titanium have been created in the aim of determine their comportment in a biomedical environment. However, their mechanical properties, and mechanical behaviour are not well defined. It seems obvious and mandatory to define them well. In fact the determination and then the data collection of them is an unmissable part of the work in order to have the more knowledge on this material before a probable use as prosthesis or other objects.

In addition, the metallurgic powder department of the Polytechnic University of Valencia have developed a SPT. In order to test it and to see if it is operational with its actual form, the determination of the properties will be done through this kind of test. In the aim of having more accurate information, and comparison for the SPT value, a second test, better known in its functioning, will be used, the microtension test.

In conclusion, the motivation of this work is to determine the mechanical properties of two pre-existing titanium alloy by a new method of characterisation.

1.4 Justification

The investigation in this field (titanium-based alloy for biocompatible material) , and with a different technique (SPT and microtension test) are justified due to a lack of information in this sphere as much for the correlation between the SPT and the microtension test as for the mechanical behaviour of theses two alloys.

Moreover, this research is justified by the first use of the Small Punch Test machine and then consequently to see if this device is well set and if it could be used with other materials.

The use of two different machines to determine the mechanical properties can also be justified by the desire to correlate the data of the SPT to the data of the microtension test and developed and give more information in this field of study which is, as said in part 1.1.2.v, a non-common field of study where there is also a lack of knowledge.

One last point, it cannot seem logical to use two different techniques to characterise the alloys. However, the amount of materials used (as the project is using microprobes) is not important, and this may be revealed, if good correlations are found, a new technique which is considered by some authors as a non-destructive method and consequently a cheap technique.

1.5 Objective

The purpose of this research is to work on two different types of titanium alloy (Titanium-Niobium-Tin and Titanium-Niobium-Zirconium-Tantalum) supposed biocompatible. In order to have a reference, the commercial titanium grade 3 have been also used. The work will focus on determining their mechanical properties, and mechanical behaviour through two different tests, the SPT and the microtension test understood before with a bibliographic part resume before in part 1.1 and in part 1.2 .

As the Small Punch Test is a new device, the first thing will to analyse the data receive from it and see if there are logical or at least explainable. During this phase of test, the exact methodology to use it will be learned in order to use it in the best condition.

After all the specimens tested, the aim of the research will be to correlate the SPT data to the microtension test data, and determine it properly if there is one. The data will also be compared between the two different alloys as they have a different microstructural composition and consequently behaviour.

Finally, in some Titanium-Niobium-Tin alloy probes some magnesium will be added, and a comparison with the simple Titanium-Tin-Niobium alloy in their comportment, and mechanical properties will be discussed.

In conclusion, the work will focus on analysing data from 2 different types of titanium alloys with a titanium grade 3 as reference obtaining by SPT and microtension test. Mathematical correlation will be investigated between these 3 different materials.

1.6 Experimental Design

In this part, the organisation of the will be done. In order to have a clear idea of the work, this part will be divided in 4 parts. The first one will focus on the preparation of the sample (for the SPT and after for the microtension test). The second part will concentrate on the utilisation of the SPT with the design of the device. In addition, in this part, the data collection will be also explained. The third part will explain all the work around the use of the microtension test. Last but not least, the description of the data processing with the software used, and the methodology used to process them will be done.

1.6.1 Preparation of sample

In order to present the preparation of the samples used during the different tests, two main parts will be explained. The first one one the Small Punch Test, and the second one on the microtension test.

i Sample of Small Punch Test

CPTi Sample

The commercial pure titanium (**CPTi**) sample was the sample of reference as its chemical composition and mechanical properties are well defined. It was the sample of "test" to see if the Small Punch device was able to work in good condition.

A cylindrical bar of $\sim$ 50 cm of length by 6 mm of diameter of CPTi was previously present in the laboratory. The aim was to create of this cylindrical bar 4 or 5 samples usable for the Small Punch Test.

As the diameter was acceptable (near from the 5 mm commonly used in this type of test) it was decided to not change it in order to gain time.

In order to reach the $\sim$ 0.5 mm of thickness required for this type of test it was mandatory to use a high-precision slicer. However, as the slicer present in the laboratory cannot handle a bar of $\sim$ 50 cm of length, a piece of this bar was previously cut with a metal saw. The titanium is known to warm up really fast while it is in friction, in order to avoid any phase changing or modification of the initial metal in the cutting area, the cutting was stopped many times in order to let time to the cylindrical bar to cool down. The length obtain from this first cutting was $\sim$ 5 cm.

After this first cutting, the $\sim$ 5 cm cylindrical bar of commercial pure titanium was set on the high precision slicer and was maintained with the cylindrical grip as shown in figure 9 .

Figure 9: Image of the bar grip for a high precision slicer

As said previously, the thickness desire was 0.5 mm. It was chosen to reach this thickness directly without polishing afterwards (as it can be done) in order to avoid any residual stress due to polishing on the small thickness. Consequently, after a first cutting (under a cooling system of the piece and the slice) of cleaning and axing the slice, the slice was set at 1 mm away (0.5 mm for the thickness of the slice and 0.5 mm for the thickness of the sample) and the cutting was done at 3000 rpm and 0.030 mm/s in a non-rotating way, in order to have efficiency and not to much warming during the cutting even with a cooling system.

After the cutting, the small disk obtain where clean (10 minutes at 35°C in a solution for ultrasound and 10 minutes in a solution of ethanol and acetone at 35°C).

After the cleaning, the burrs present due to the cutting were washed away with a P1000 grinding paper by hand in order to generate the smaller possible stress on the sample. The image 10 gives a comparison in size between the probe and a piece of 20cts. This image shows also the general shape of a SPT probe of CPTi.

Figure 10: Image of a CPTi probe of SPT in comparison with a piece of 20cts

TNS Sample

The Titanium-Niobium-Tin (**TNS**) alloy was at the contrary of the two other samples not already existing in the laboratory. This sample was fabricated for this experiment, but also for a global analyse of it, which means for the biomedical analysis, its corrosion resistance and the global analysis of its mechanical properties. In this aspect, it seems interesting to explain how the material was created in order to give more information for a potential other development of this research.

The solid material was fabricated from powder as the investigation occurs in the metallic powder laboratory. The exact mass of each component (Titanium, Niobium and Tin) where measure with a high precision scale in a neutral and control atmosphere in order to avoid any contamination (especially oxidation of the pure titanium). Of the predefined chemical composition, ~ 1.5 $\%wt$ of NaCl in powder have been added. The NaCl works as a dispersing agent in order to increase the homogeneity of the piece created.

After the exact composition weighing and noted, the preparation is mixed without being in contact with the atmosphere in a rotate machine for at least 40 minutes. This enables to have a homogeneity in the mixture of the powders.

After the mixture, it was desired to create a physical change of phase through milling. In order to create this phase changing, it is mandatory to have a mechanical action on the powder with enough time to do it. For that, a milling machine was used and the mechanical action was applied through a cinematic (centrifuge) force applied on steel balls which are in contact with the powders. The powders and the steel balls have been putted in a 450 mL jar. It is recommended to put 10 times the weight of the powder in steel balls. The radius of the balls were between 2 mm and 3 mm. The milling process last 72h. In this 72 hours there was 40 hours of milling and 32 hours of rest in order to avoid the friction and the warming up of the powder as the phase changing must occur thanks to a mechanical action and not a thermal action. These parameters have been studied before by the laboratory and seem the optimal parameter.

The all process must occur under a control atmosphere, in order to have a neutral atmosphere, argon was putted in the jar (two times: one filling then one vacuum, and one time one filling). In the aim to be sure that the process was in a controlled atmosphere during the all time, each 24 hours, a vacuum and filling with argon of the jar where made. If during the vacuum there was not gazes ejected, it was the sign of a non controlled atmosphere.

After this 72h, the powder is extracted from the jar (it has to be done cautiously the powder can inflame itself instantly). After this process, the sintering of the powder is done. The dry powders were compacted at 100 or 200 MPa during 15 secondes. The sintering occurs in a high vacuum resistive furnace coupled to mechanical pumps and diffusers. The sample chamber was pre-purged with argon and heated at 450°C for 2 hours. Depending of the sample, some have been pushed under 900°C or 1100°C with 2 hours as stop time.

The embedding used was made of a transparent resin (TransOptic, Bhuler) for 210 secondes of heating and under 350-bar pressure and then 6 minutes for heating and cooling under water.

From the sintering process, rectangular blocks of Titanium-Niobium-Tin alloy were obtained. In the aim of saving time, and see the comportment of this type of geometry, the decision of having rectangular sample instead of circular sample was made. One thing which has led to this decision was the fact that the smaller dimension of the rectangle was bigger than the hole of the base of the SPT device, and consequently will not create an accumulation of stress on the sample.

Consequently, and after a short discussion on it, the cutting process was carried out. The cutting was made by the high precision slicer with a consumable slice because the diamond slice was broken. A first cutting in order to clean the sample was mandatory due to the fact that the samples have suffered a thermal process. In addition, this first cut enables the slice to be perfectly parallel to the sample and consequently having specimens perfectly straight. As, the work was carried out with a consumable disk, the perpendicular speed of the disk was smaller: 0.010 mm/s at 3000 rpm. For each specimen, the disk was set at 0.945 mm of distance from the end of the sample for having a thickness of 0.5 mm (0.5 mm desired + 0.445 mm thickness of the consumable disk). The cut was proceeding under a cooling system as for the CPTi sample.

A cleaning of the sample after the cutting was made (10 minutes at 35°C in a solution for ultrasound and 10 minutes in a solution of ethanol and acetone at 35°C). For these samples, a bigger burr was present (maybe due to the geometry of the piece). It was consequently very important to take them off. As for the CPTi sample the burrs were taken of thanks to grinding paper, first with P500 and then with P1000, the grinding process was made by hand. The figure 11 shows an image of the TNS probe for the SPT with a scale in order to have an idea of the size of the probe.

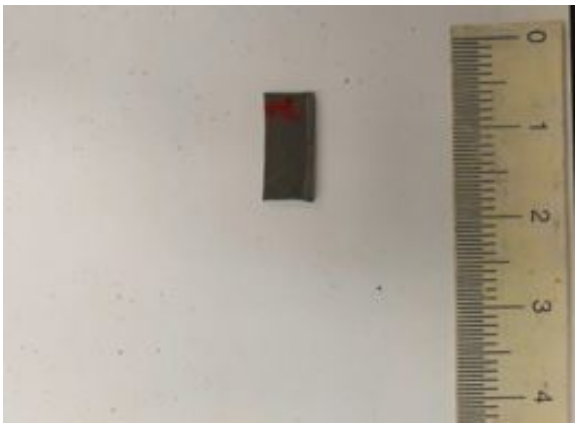

Figure 11: Image of a TNS probe of SPT, the graduations are in cm

TNZT Sample

The preparation of the Titanium-Niobium-Zirconium-Tantalum is quite similar as the one of the CPTi. In the laboratory a cylindrical bar of this alloy was present (see figure 12). The bar was ~ 5 cm of length by 11.40 mm of diameter. This diameter is much bigger as the two previous one. However, as it fitted perfectly in the device system, the decision to let it with this dimension was made in order to gain time.

Figure 12: Image of the TNZT bar present in the laboratory

This sample was shorter in length than the one of CPTi, so the sample could be directly cut under a cooling system as the previous one. The parameters of the high precision slicer were the same, which means: 3000 rpm and 0.030 mm/s. However, as the diameter of the bar was bigger, and in order to save some time, the process was on rotating mode, which enables to cut 2 times faster. In addition, due to the fact that the diamond slice used previously for the CPTi was broken, a consumable slice was used to cute the 5 samples as for the TNS sample.

After the cutting process, as for all the samples, a cleaning process was made following the same methodology as the other sample (10 minutes at 35°C in a solution for ultrasound and 10 minutes in a solution of ethanol and acetone at 35°C).

After the cleaning, the burrs (present in the middle of the probes due to the rotating cutting) were taken away thanks to a grinding paper of P1000 by hand.

ii Sample of microtension Test

In this part, only TNS probes have been tested (the TNZT probes were already tested) so consequently, only TNS probes have been prepared from the same block of metals as previously prepared.

The preparation of the probes were made by a CNC milling machine. The mechanisation was made following the norm ASTM A371 through a program made from the G code.

The milling machine used was 5 mm of diameter with 4 cutting string. The cutting speed used was 20 mm/min with a revolution of 900 rpm.

After all the machining of the probes, two white points were glued on the probes at the beginning of the neck and the end of the neck in order to be able to measure the displacement or stress of the probes through an optical technique.

1.6.2 X-Ray Diffraction analysis

The X-Ray Diffraction (XRD) analysis is an important part in order to study the mechanical behaviour of a material through its microstructure.

The methodology used is well known, however it seems always good to remind it.

A Cu $K\alpha$ radiation was used and works at 30kV and 10mA. The measurement was made between 20 degrees to 90 degrees with a step value of 0.02° every 10 secondes. The refinement of the structure and the quantitative phase analysis were carried out through the software MAUD (version 2.94).

1.6.3 Small Punch Test

This part will explain the methodology use for the Small Punch Test. It is important to note before reading this part, that it was the first time that this machine was used in this laboratory.

Before to start with the methodology, a short digression on the device system is done. The device has been created in the laboratory following the dimension showed in the part 2.2.4 following the thesis made by Avila, 2019. First using a CAD software, Solidworks, to generate plans for the conception of the device. Afterwards, the conception of it has been done in another laboratory of the Polytechnic University of Valencia.

The first thing is to set the rod on the top grip. After, the sample is set in the hole of the base, and thanks to screw fixed and maintain with the upper part. It is very important to screw carefully and applied a homogeneous force on the sample otherwise the test will not occur in good condition. Many times if the upper part screwed is not perfectly parallel to the base, the test was carried out in a wrong way and the curve obtain was wrong.

After the sample set, the ball of steel of 2.4 mm of diameter is set through the upper hole in the middle of the probes. Afterwards, the all set up was putted under the rod and align with it in order to have a coaxial force.

Then, the test can be started, at normal atmosphere, ambient temperature and constant velocity (0.5 mm/min). The force is applied by the upper grip on the rod and the value of the displacement and force are at the same time measured by the software. As for the microtension test (see part 1.6.4) it is possible to obtain some value from the software. The typical force displacement curve is shown in figure 3.

After the test realised, the all set up was taken off (it is mandatory to be carefully with the ball which can be at the end of the rod). The screws were taken off carefully, and the sample can be extracted. The sample has normally the aspect of the one in the figure 13.

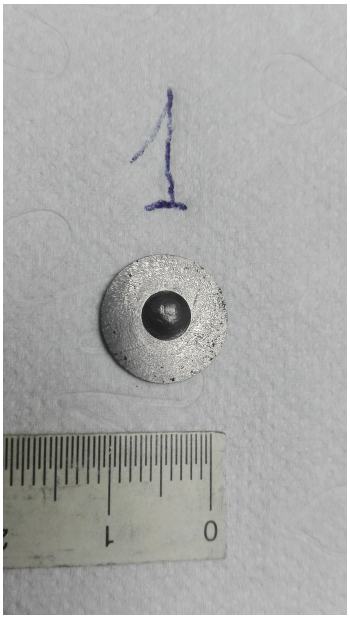

Figure 13: Image of the CPTi-1 probes after the SPT

1.6.4 Microtension Test

In this part, the methodology used to do the microtension test will be explained.

Firstly, it is important to measure correctly the dimension of the probes obtain from the previous machining. The thickness and the depth of the useful zone (the zone which is situated in the middle of the neck of the probe in order to follow the *Saint Venant* principle). Last, but not least, the length between the two white marks is measure. This length was measured at the end of the one mark and the beginning of the second one in order to diminuate the size effect of the marks.

After all the dimension measured, the test can start. It is quite similar as a bulk size tension test. First, the sample is set up in the machine and attached by the grip. After the dimension set in the software, the test can start. A load is applied and noted while a stress is occurring and thanks to the optical method measured. In the figure 14, it is possible to see the typical stress/strain deformation. All the tests occur at the same velocity (1 mm/min) at normal atmosphere and ambient temperature. Thanks to the software it is possible to reach some values really easily as the slope between 2 points (and consequently the Young's Modulus), the maximum of stress, strain, the σ_y and the $0.2\%\sigma_y$.

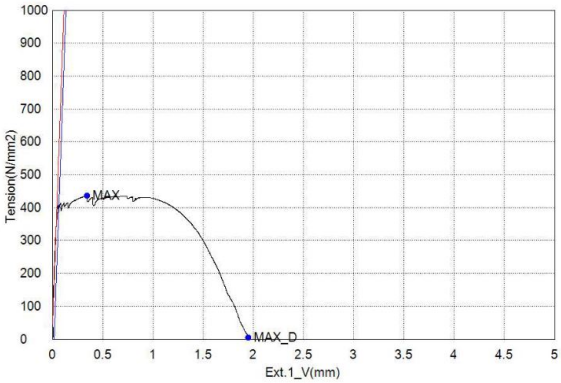

Figure 14: Image of a typical tension curve obtain on the TNZT-1 sample

At the final of the microtension test, the length of the probes is noted, and the data are saved in different forms in order to be sure to be able to reuse, recalculate them without problems. The figure 15 and the figure 16 show the sample before and after the test.

Figure 15: Image of the microtension sample before the Test

Figure 16: Image of the microtension sample after the Test

1.6.5 Data processing

In this part of the report, the data processing of the sample (the XRD and the measurement analysis), the data processing of the SPT and of the microtension test will be explained.

i Data processing of the Sample

For the TNS and TNZT it was possible to determine their phase in presence thanks to a XRD analysis.

In order to analyse the XRD data from the TNS and TNZT after the milling process, the software "Maud" was used. This software enables, through comparison of previous data from "icsd-bases, to get the different phases of the sample, its crystalline plan and the composition of the sample.

From the samples themselves, excepted their aspect and their dimension no more information could be extracted. The dimension of the SPT sample expected are the thickness of the probes, because the diameters were previously known. Theses thicknesses were measured by a high precision measurement device. Afterwards, all the thicknesses were measured and a mean and the standard deviation could be calculated for each group of sample.

For the microtension test, the area and the length were measured with a high precision electronic calipers. As for the SPT, the mean and the standard deviation could be calculated.

ii Data processing of the SPT

Before any data processing of values, photography of each sample after SPT by optical microscope with a adequate magnification was made.

In order to process the data of the SPT, the software Excel was used as much as the software Trapezium X which is the software from the TENSION machine.

As said previously, from this test, different methods to obtain the P_y value can be used. From the different software, two different P_y value have been obtained.

The P_y value obtain from the software of the machine that in this report will be called the P_y^{offest} is similar as the offset method previously presented in this report. This value is the intersection between the force-displacement curve and the parallel of the slope of the region I. In order to have a point to be able to trace this second curve, the value of x corresponds to a relative elongation $\epsilon = 0.2\%$. Nevertheless, other important values such as the maximum force and its respective displacement have been obtained from this software. Consequently, from the software Trapezium X pdf pages such as in figure 17 have been obtained.

Nombre	LE1_Fuerza	LE1_Desplazamiento	Pend._dos puntos	Max._Fuerza
Parametros	0,2 %	0,2 %	Fuerza 200 – 400 N	Calc. at Entire Areas
Unidad	N	mm	N/mm	N
TiCP-2	534.185	0.28283	2230.72	1157.16

Nombre	Max._Desplazamiento
Parametros	Calc. at Entire Areas
Unidad	mm
TiCP-2	0.87108

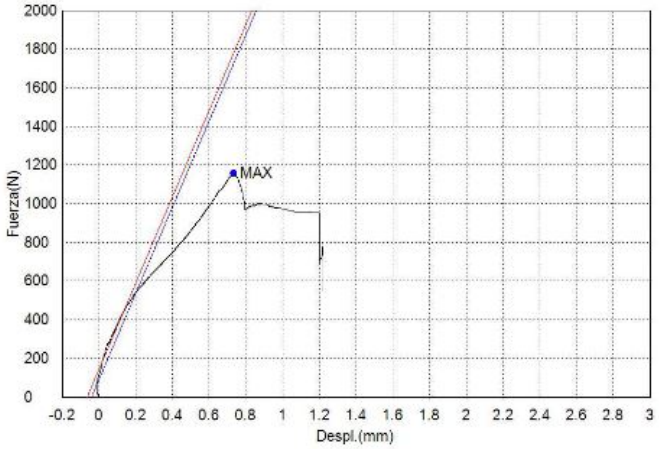

Figure 17: Image of the CPTi-2 analyse through the software Trapezium X

In order to obtain the other values, such as the P_y^{CWA}, which corresponds to the value of that the CEN recommend, the data were extracted in Excel format from the device system and could be consequently directly analysed.

For each sample, the curve force-displacement was traced, the elastic zone was distinguished from the plastic zone and from them, then the linearisation of the part I and the part II were made in order to be able to have the intersection of them and the reach the intersection value with the Force-Displacement curve.

The figure 18 shows the curve and the intersection in order to obtain the P_y^{CWA}. The figure 19 is a zoom of the part in order to see that the value is not exactly the intersection between the 2 tangents.

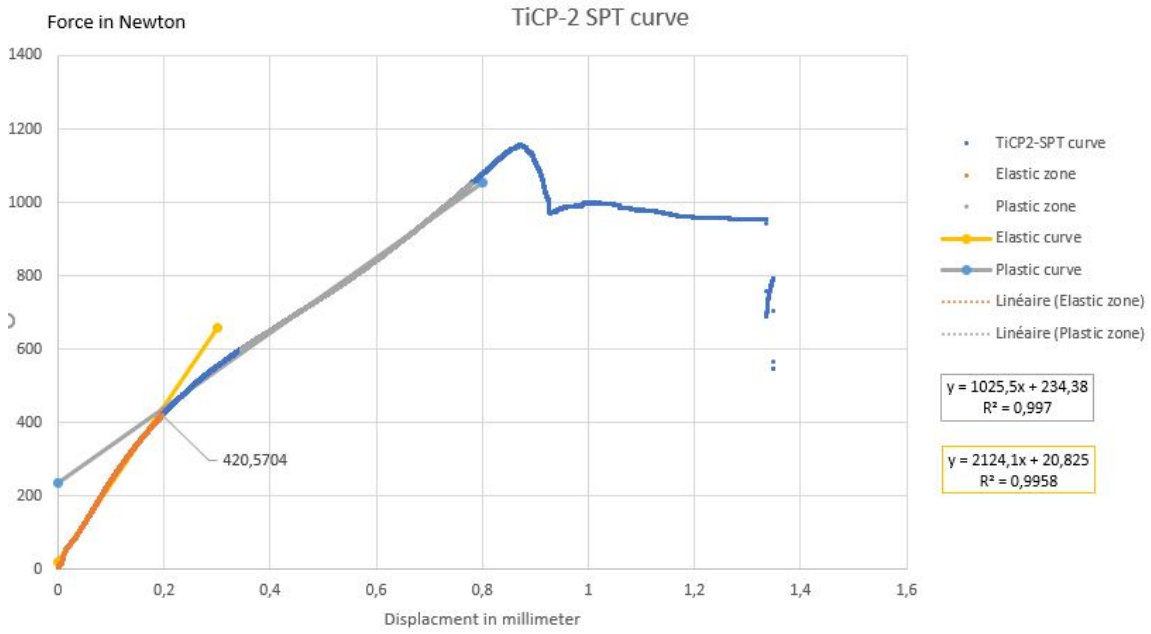

Figure 18: Image of the Force-Displacement curve of the CPTi-2 probes done on Excel

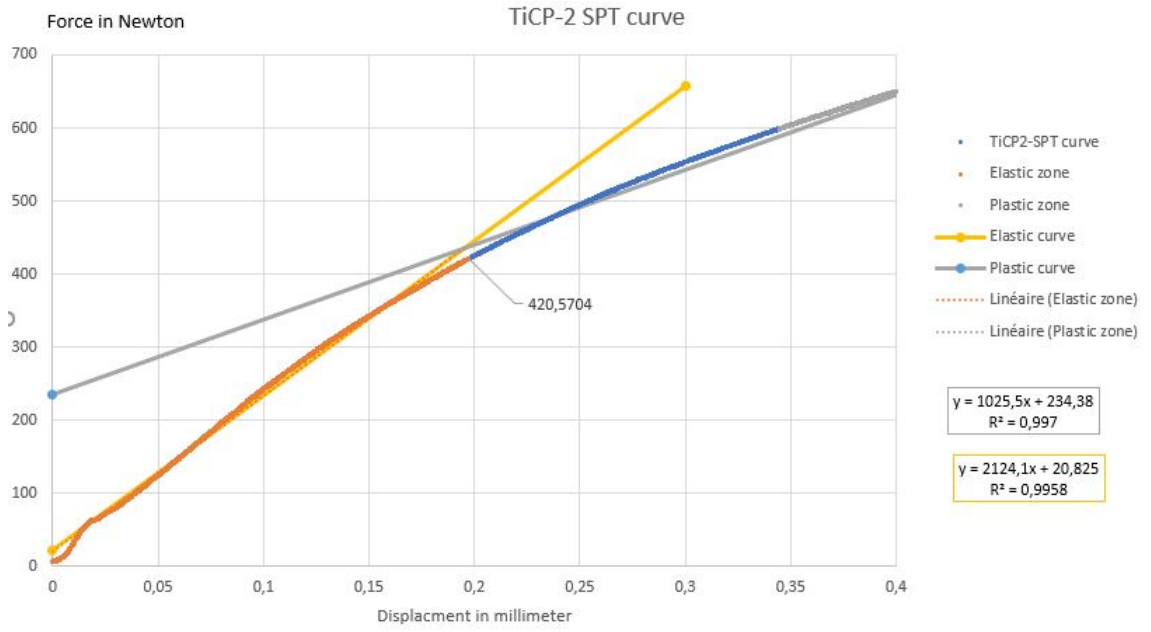

Figure 19: Image of a zoom of the Force-Displacement curve of the CPTi-2 probes done on Excel

As said previously, this was made for each sample, consequently the mean and the standard deviation could have been calculated for each family of sample.

However, Excel nor Trapezium X can't calculate properly the derivative and the area under the curve. In order to calculate them and obtain consequently the energy, the F_c and z_c, the software Origin was used.

To calculate the derivative, firstly as there was too many points and variations between them it was impossible to clearly read the curve. It was consequently decided to smooth the curve. The methodology used was the following. First, smooth the curve with the Savitzky-Golay Method by order 1 or 2 depending of the curvature of the curve with a value of 200 for the Points of windows. After the smooth done, the derivative was calculated on this smooth curve by the Savitzky-Golay Method at the order 1. Then, when the derivative curve was traced on the same graph that the force-displacement curve, the F_c and z_c values were determined graphically thanks to a cursor. The typical curve obtained on Origin is shown in figure 3

For the energy, a simple integration of the curve was able to give a value of the energy.

iii Data processing of the microtension test

In the aim of process the data from the microtension test, the same software as for the SPT were used. From the software Trapezium X, the maximum strength, maximum stress, the value of the slope (equivalent of the Young's Modulus), the $0.2\%\sigma_y$ (also call Re0.2) and its respective stress were obtained. For having the σ_{uts} and ϵ_u, the software Origin was used. It was previously desired to obtain as for the SPT by a smoothing and then a derivative. However, this technique has not been able to be used. In order to have some data, a new methodology have been developed.

This new technique consists of smoothing the curve in order to avoid big variation between the following points as done previously. The smooth was made with another technique, call Adjacent-Averaging Method with a points of Windows value equal to 1500. Afterwards, the derivative was calculated by the mathematical formula dF/dz.

This method enables to get some value of the intersection as it is possible to see on figure 20.

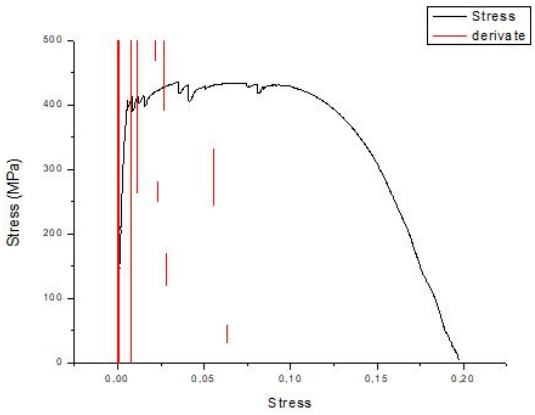

Figure 20: Image of the Stress-Strain curve of the TZNT-1 made by Origin with its derivative

All the values were afterwards, process on Excel in order to have a mean and their standard deviation.

2 Material and methods

In this part, the chemical composition of the sample will be explained and described. In addition, the machine used for the project will be shown and described with their accuracy and dimension.

2.1 The probes

2.1.1 Chemical composition of the probes

As described in part 1.6, 3 different types of sample were used. The CPTi (Commercial Pure Titanium), the TNS (alloy of Titanium, Niobium, Tin) and the TNZT (alloy of Titanium, Niobium, Zirconium, and Tantalum). In this part, the chemical composition of the sample will be described.

The chemical composition of the probes of the SPT and microtension test are the same, that makes more sense in order to compare the 2 different techniques.

The CPTi used was a grade 3 commercial titanium. On internet, it is possible to find its chemical composition (Boyer et al., 1996; Institut für Auditierung und Zertifizierung GmbH, 2014), the table 1 gives the chemical composition of it. The percentages are in weight.

Table 1: Table of the chemical composition of the CPTi grade 3

C %wt	N %wt	Ti %wt	Fe %wt	O %wt	H %wt
≤ 0.08	≤ 0.05	Rest	≤ 0.30	≤ 0.35	≤ 0.015

The TNS sample, as said previously have been created in the laboratory. The alloy desire was a $Ti - 34Nb - 6Sn$. The table 2 resume it. After this mixture, $\sim 1.5\%wt$ of NaCl have been added. This is the disperse agent of this alloy, this agent is important to have a homogeneity in the composition of the sample.

Table 2: Table of the chemical composition of the TNS

Ti %wt	Nb %wt	Sn %wt
60	34	6

The purity and the size of grain of the powder is given in the table 3.

Table 3: Table of the purity and size of the grain

Element	Ti	Nb	Sn	NaCl
Purity	99.70%	99.80%	99.80%	99.50%
Size in μm	44	1-5	44	

From this mixture, the sintering process has been carried out on different conditions. Theses conditions are summarised in table 4. In some sample, the TNS-3, TNS-6, TNS-7, TNS-8, some magnesium (3%wt) have been added (that is why in their composition there is "-m") in order to evaluate the microstructural and mechanical properties with magnesium.

Table 4: Condition of the sintering process

Name of the sample	Temperature in °C	Compaction in MPa	Chemical composition
TNS-1	900	100	TNS
TNS-2	1100	100	TNS
TNS-3	1100	100	TNS-m
TNS-4	900	200	TNS
TNS-5	1100	200	TNS
TNS-6	900	200	TNS-m
TNS-7	1100	200	TNS-m
TNS-8	900	100	TNS-m

The TNZT was processed by casting under vacuum. The cylindrical sample was cut by the company Biomet Ibérica. S.A. using the electrospinning. Its chemical composition is resumed in the table 5. The percentages are in weight.

Table 5: Table of the chemical composition of the TNZT

Ti %wt	Nb %wt	Zr %wt	Ta%wt
53	35	7	5

However, as the material was already present in the laboratory, the purity of the powder cannot be summarised.

2.1.2 Geometry of the probes

i Dimension of the SPT probes

After the cutting, the thickness obtained was nos exactly the same for all the family of sample even if the cutting process was done cautiously . In the aim of having a clear idea of the different thickness the table 6 resume all the thickness of the CPTi probes. The diameter of all the CPTi samples were 6 mm.

For the TNS sample the table 7 resume the thickness of all the samples, their diameter were supposed constant and equal to 4 mm (the size of the hole of the base (Dp)). The values given in the table 7 are the thickness and they are in millimeters .

For the TNZT sample, the thicknesses of the disks are resumed in table 8, and the diameter for all was 11.40 mm.

Table 6: Table of the geometry of CPTi SPT probes

Name of the probe	CPTi-1	CPTi-2	CPTi-3	CPTi-4
Thickness in mm	0.440	0.427	0.434	0.440

Table 7: Table of the thickness of TNS SPT probes

Name of the probe/N° of the probes	TNS-1	TNS-2	TNS-3	TNS-4	TNS-5	TNS-6	TNS-7
1	0.575	0.559	0.544	0.446	0.762	-	1.199
2	-	0.506	0.525	0.683	0.525	1.094	0.911
3	-	0.535	0.665	0.535	0.532	0.591	0.305
4	-	0.595	0.557	0.517	0.499	-	0.446
5	-	0.641	0.442	0.473	0.797	0.575	0.494

Table 8: Table of the geometry of TNZT SPT probes

Name of the probe	TNZT-1	TNZT-2	TNZT-3	TNZT-4	TNZT-5
Thickness in mm	0.788	0.687	0.612	0.647	0.555

ii Dimension of the microtension test probes

In this part, the dimension of the microtension Test probes will be summarised. As explained previously, the value of the microtension test for the CPTi was the value from internet in order to have an accurate value of its mechanical properties in order to have a reference. However, it is important to have the value of the other samples.

For the TNS, the dimension of the microtension test probes have been summarised in the table 9. The thickness and depth have been measured in the middle in the useful zone, while the initial length has been measured between the beginning of the first mark and the end of the last mark in order to take into account the variation of the thickness of the mark. For the TNZT the dimension are given in table 10.

Table 9: Table of the geometry of TNS microtension test probes

Name	Number	Thickness (in mm)	Depth (in mm)	Initial length (in mm)
TNS-1	A	1.50	2.15	-
TNS-1	B	1.25	2.17	-
TNS-1	C	1.50	2.07	10.68
TNS-1	D	1.48	2.06	10.01
TNS-2	A	1.35	1.94	10.89
TNS-2	B	1.35	1.92	9.86
TNS-2	C	1.65	1.93	10.63
TNS-3	A	0.87	2.07	9.67
TNS-3	B	0.78	2.26	10.53
TNS-3	C	1.40	2.28	10.18
TNS-3	D	1.90	2.16	10.43
TNS-4	A	0.63	2.01	9.64
TNS-4	B	1.59	2.17	10.65
TNS-4	C	1.53	2.08	10.09
TNS-4	D	1.43	2.02	1.08
TNS-5	A	0.84	1.93	9.29
TNS-5	B	1.3	1.94	10.07
TNS-5	C	1.16	1.94	10.22
TNS-5	D	1.23	1.94	10.27
TNS-7	A	1.27	2.23	10.35
TNS-7	B	1.88	2.13	10.31
TNS-7	C	2.27	2.19	9.71
TNS-7	D	1.22	1.95	9.76
TNS-8	A	1.16	2.2	9.24
TNS-8	B	1.28	2.16	10.25
TNS-8	C	0.86	2.99	10.64

Table 10: Table of the geometry of TNZT microtension test probes

Name	Thickness (in mm)	Depth (in mm)	Initial length (in mm)
TNZT-1	1.60	2.10	9.89
TNZT-2	1.50	2.11	9.87
TNZT-3	1.50	2.02	8.80
TNZT-4	1.50	2.11	8.84
TNZT-5	2.80	2.08	9.19

It is important to note that the TNS-6 has not been tested by the microtension test and the TNS-8 by the SPT.

2.2 Device used

It is important to have an idea of the machines used during the project and if the accuracy of the devices is known it is as much important to have their values in order to be able to have an idea of the accuracy of the results. This part will present all the devices used.

2.2.1 The measurement device

In order to measure the samples and have the thicknesses and length of all, two types of measurement system have been used. The first one: a Mitutoyo digimatic indicator ID-C150B with a resolution of: 0.001 mm. This system was used in order to measure the thickness in the middle of the probe for the SPT.

For the microtension test probes, an Electronic Digital Caliper 0-150 mm, with a resolution of 0.002 mm was used. All the dimensions of the microtension test probes were measured with this system.

2.2.2 The devices used for the creation of the probes

In order to create the bloc of probes before a machining, a mixer (planetary mill PM400/2 of Retsch) was used. The mixing time needs to be more than 40 minutes. And with theses types of mixer, the mixing is a rotated mixing. The figure 21 shows the machine.

After the mixing, the milling was process through the INversina 2L of Bioengineering machine. The figure 22 shows the milling machine used for change the phases of the powder.

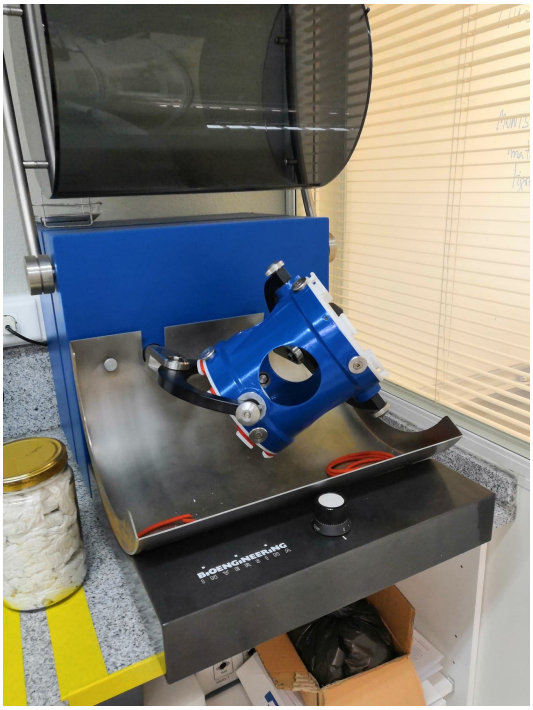

Figure 21: Image of the mixing machine used

Figure 22: Image of the milling machine used

The furnace used for the sintering process is a COMBUSTOL- tube furnace model coupled to mechanical pumps and diffusers (EDWARDS).

During the machining of the SPT probes the slicer use was a Acutom 10 of Struers, and a diamond disk and a MOD 13 disk were used. The accuracy of the disks which are their size are the following one: 0.5 mm for the diamond and 0.445 mm for the combustible one made of MOD 13. The device using for the machining of the microtension test was the Optimum model BF20L Vario.

The ultrasounds machine used to clean the sample after the cutting was the ELMASONIC S30 H.

2.2.3 Devices used for the characterisation

There was two different devices that enables to characterise the probes. One before the test was the XRD device, and the second, the optical microscope, one after the SPT in order to study the fracture.

The XRD device was the BRUKER/2D Phaser analyser, and the optical microscope was the Optical Nikon-ECLIPSE LV100 DA-V.

2.2.4 The SPT device

As said previously, the SPT used have been created in the Polytechnic University of Valencia. The figure 23 shows the SPT device in its wholeness. On the right of the image, the rod and on the left, the fixation. On the top a scale, the unit is the centimeter. The exact dimensions of the device are given in the appendix A.

The ball used during all the tests, was made by steel and its diameter was 2.4 mm. For all the tests, the same ball was used.

Figure 23: Image of the SPT device used for the test. The scale is in cm.

2.2.5 The microtension test device

The device used was adapt from the tension test machine (Shimadzu Autograph X-Plus 100 Kn).

As said previously, different types of grip, of fixturing system exists. Here, a clamping system was used. The deformation was measured by an optical method with the software Trapezium X in order to have the deformation only in the useful zone and not for the all sample and in the aim to minimise the deformation of the crosshead itself too.

3 Results

The results of the project will be shown in this part, starting with the XRD analyse in order to identified the phases present in the sample and their percentage. Afterwards, the results of the Small Punch Test and the photography of the fracture will be shown. Thirdly, the results of the microtension test will be resumed and last but not least, the correlation of the value of SPT and microtension which was the aim of the project was made.

The results obtain are the means of the family of sample, in the aim of reducing the number of values, graphs and photography, only some representative figure will be in this part. However, all the values, graphics and photographs are in the appendix B.

3.1 XRD of the powder

3.1.1 CPTi sample

None XRD analysis have been made on the CPTi grade 3 samples. However, as the sample is Titanium commercial pure 3, its main composition phase is the α phase.

3.1.2 TNS sample

The XRD analysis of all the probes of TNS have been made. Figure 24 and figure 25 show the XRD graphs of the sample. The nomenclature used is the same than for the sinterering parameter and it will be the same for all the report. As for the half of the TNS probes magnesium (3%wt) have been added at the chemical composition, the XRD graph are divided into two groups. The first one without, and the second with magnesium.

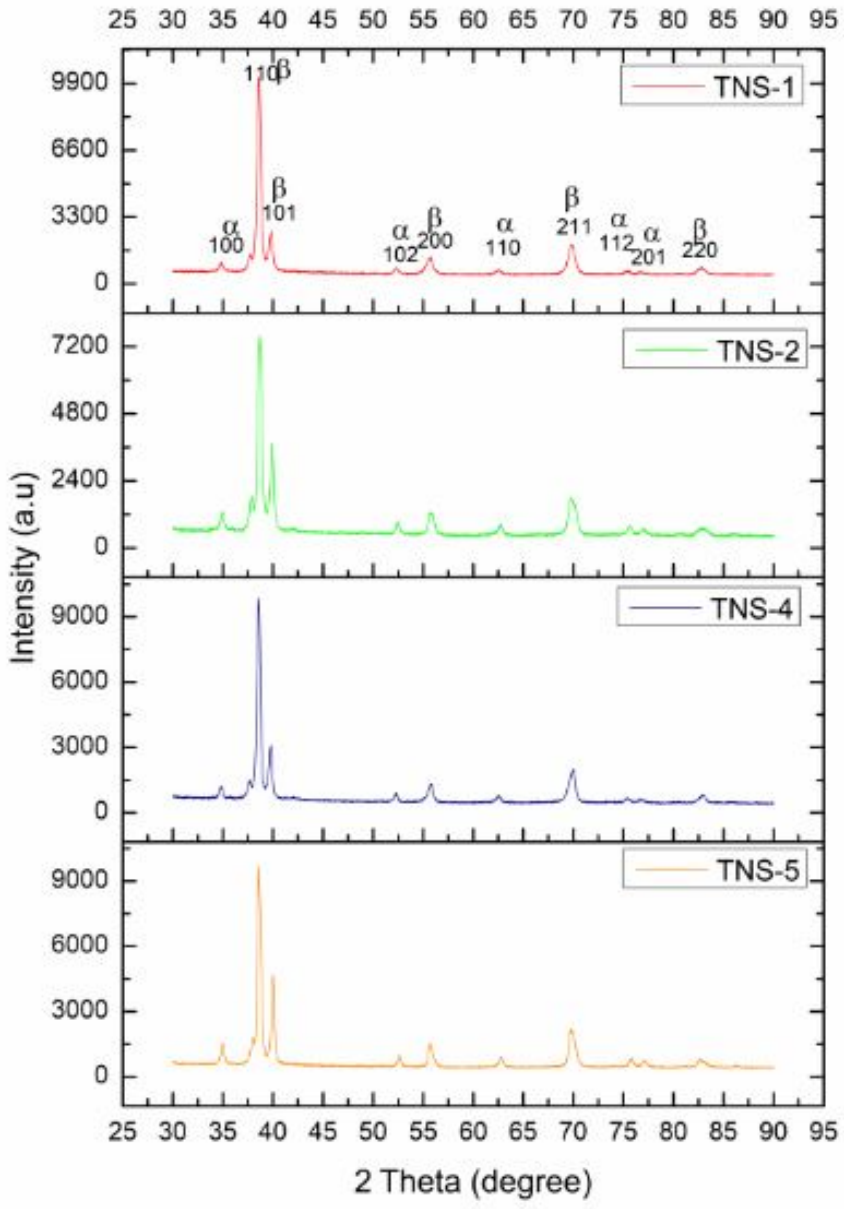

Figure 24: Image of the XRD analysis of TNS without magnesium

The crystalline plan and the nature of the phase are given for each pics in the first XRD graph, they are respectively the same for the other pics of the other graphs.

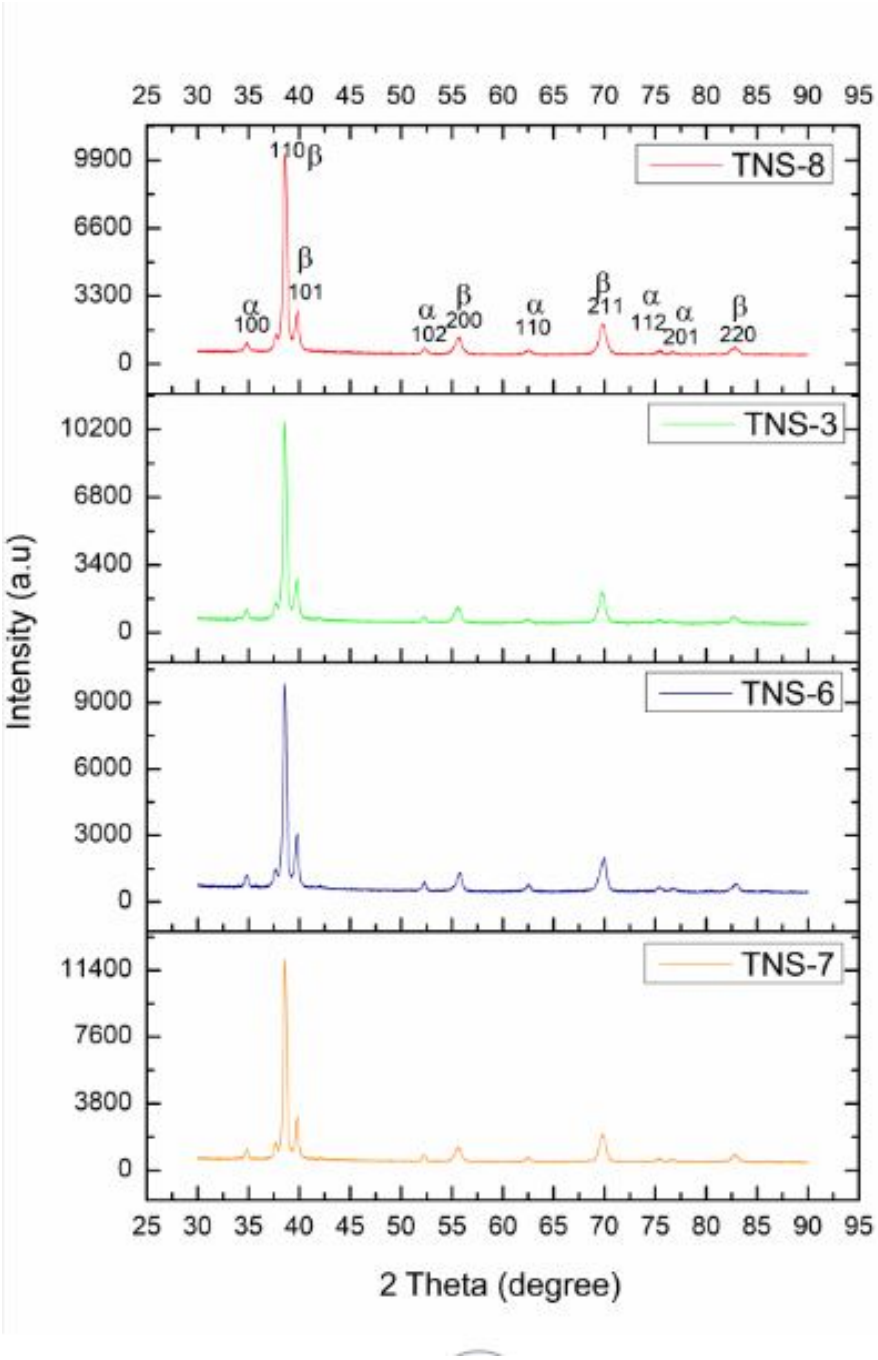

Figure 25: Image of the XRD analysis of TNS with magnesium

It is important in this case to notice that the niobium has mesh parameter close to the β phase of the titanium, this induce difficulty for the software to distinguish both and then, consequently it can have a effect of the analysis.

3.1.3 TNZT sample

The XRD of the TNZT alloy have been made in previous research. The graphical of the XRD is shown in figure 26.

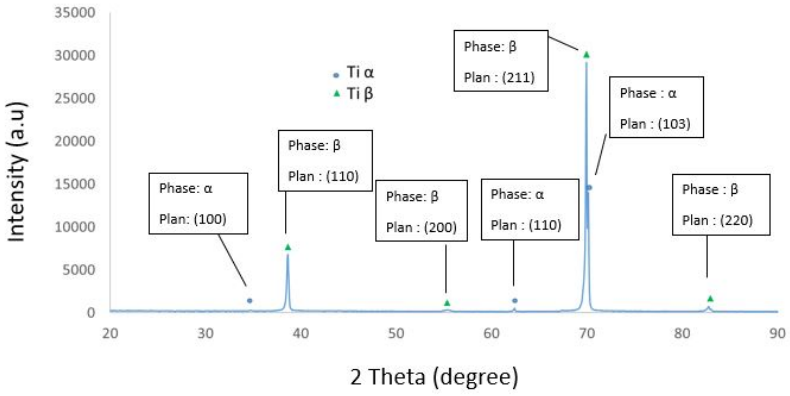

Figure 26: Image of the XRD analysis of TNZT probe

3.2 Small Punch Test values

3.2.1 Mechanical values of the SPT

In the table 11, all the results of the SPT test are resumed. The values are rounded to 10^{-2} and are the means of the family of the probes. In the appendix B, all the results of the samples are given. As for the family of sample TNS-7, there was 2 really different size, it was decided to split their results in 2 only for the correlation with σ_{uts} see part 3.4. The ones where the thicknesses were $< 0.5mm$ (TNS-7.2) and the 2 other ones where the thicknesses were $> 0.9mm$ (TNS 7.1).

For each, sample the SPT curve was made on Excel in order to have the value of the slope, and the P_y^{CWA}. The SPT curve was also traced on Origin in order to have the P_c and z_c value. However, as the values have not been used for the correlation there are not present in the table 11. The figure 7 shows the curve on Origin, and figure 18 the figure and 19 show the curves made on Excel. All the other curve are on the appendix B.

Table 11: Table of the means values of the SPT probes

Properties	CPTi	TNS-1	TNS-2	TNS-3	TNS-4	TNS-5	TNS-6	TNS-7.1	TNS-7.2	TNZT
P_y^{offest} (N)	428.66	260.97	145.53	185.76	99.87	253.04	221.3	443.39	-	240.20
P_y^{CWA} (N)	490.67	-	119.75	114.11	73.86	136.57	203.032	423.91	18.63	242.13
$Slope^{inti}$ (N/mm)	2107.25	2207.2	1779.58	1336.84	1115.35	2023.96	1804.8	2874.95	583.32	2025.46
Pmax (N)	1207.10	319.45	174.27	235.56	118.92	276.40	359.32	606.44	30.86	1535.86
Zm (mm)	1.00	0.41	0.189	0.49	0.18	0.33	0.44	0.39	0.17	1.93
Energy ($N * m^{1.5}$)	828.78	308.79	71.22	127.26	41.31	138.73	243.71	397.41	10.56	2203.106

3.2.2 Fracture of the probes

In this part, photography of the probes after the test in order to see more clearly the fracture and deformation have been done.

The figure 27 show the CPTi probes after the SPT. The scale (at the top left of the picture) is 1 mm.

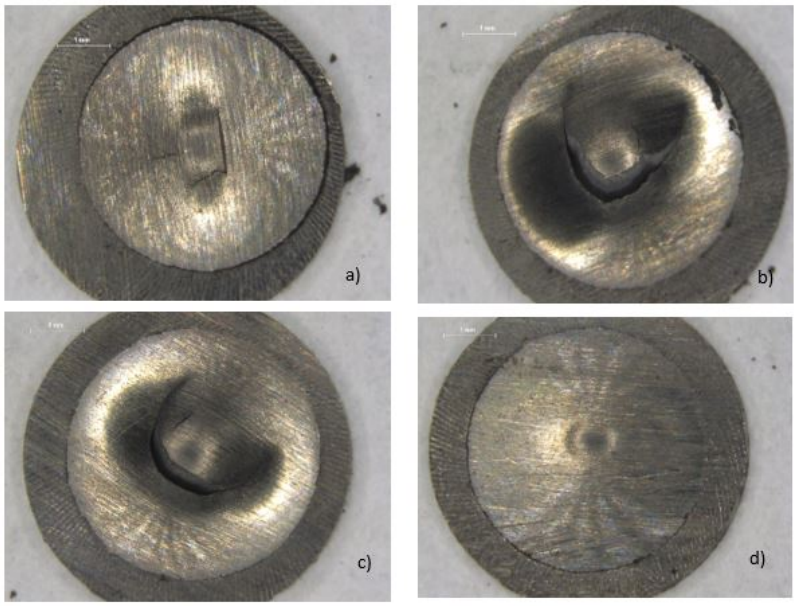

Figure 27: Image of the CPTi probes after the SPT. The image a), b), c) and d) correspond respectively to CPTi-1, CPTi-2, CPTi-3 and CPTi-4

The figure 28 shows the TNS-4 samples after the SPT. The TNS-4 probes were created without magnesium. It is also possible to see more clearly the geometry of theses probes, the rectangular one in comparison with the one of CPTi. The scale (at the top left of the picture) is 1 mm.

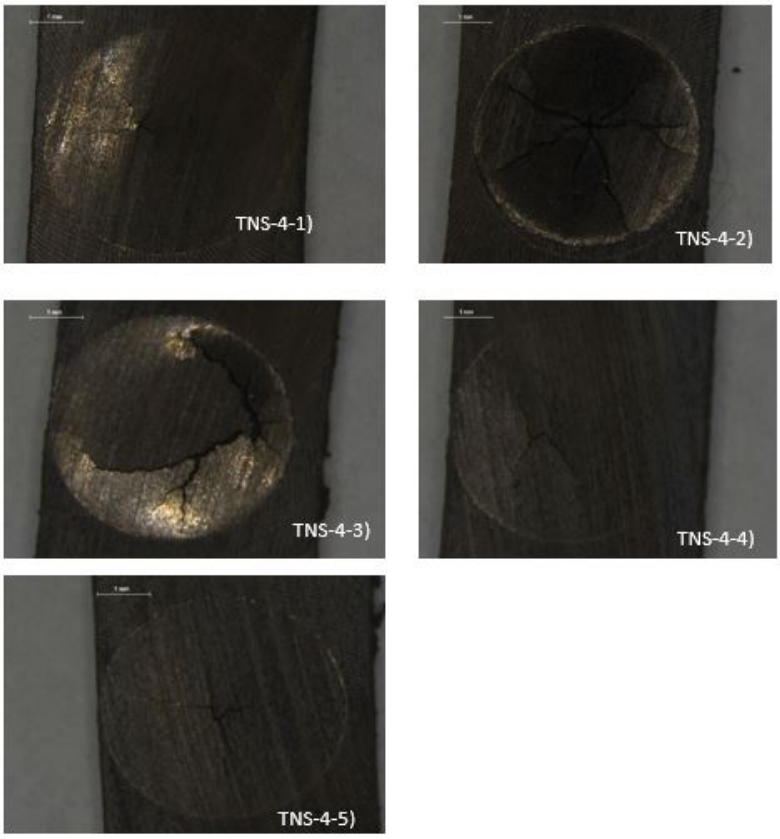

Figure 28: Image of the TNS-4 probes after the SPT

The figure 29 enables to see the TNS-7 probes after the SPT. It is important to note that the TNS-7 samples were made with magnesium. As the TNS-7.3 have not given good results (it is possible to see that the deformation has not been well done) their results were taken out for the calculus of the means. The photographs of all the samples enable to see the centring of the punch through the ball on the sample. The scale (at the top left of the picture) is 1 mm.

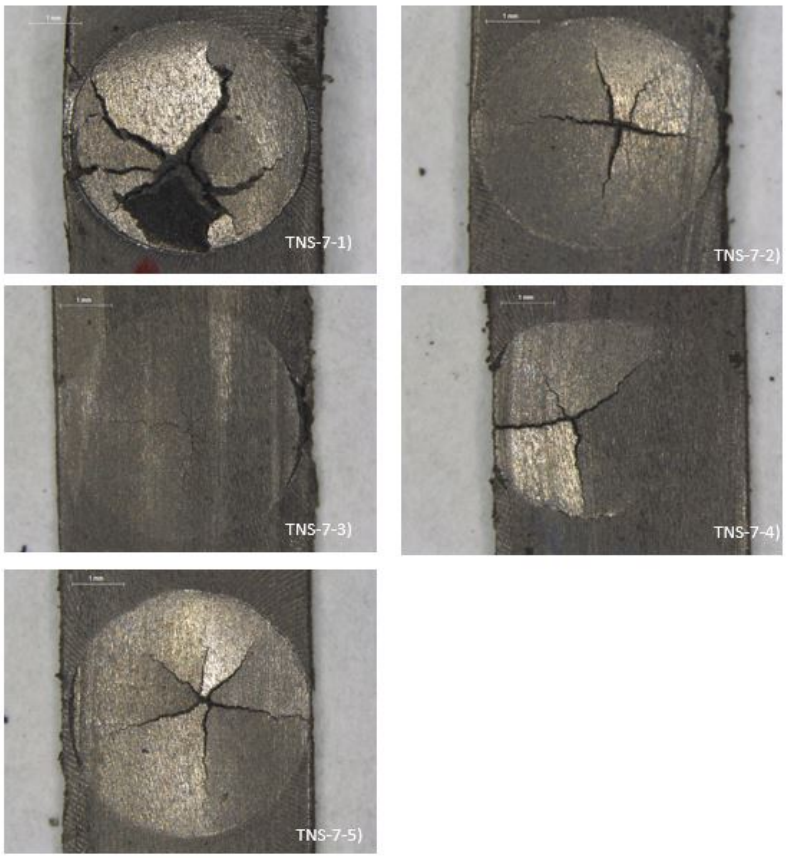

Figure 29: Image of the TNS-7 probes after the SPT. The TNS-7 has magnesium

3.3 Microtension test values

The results from the microtension test are resumed in the table 12. As for the SPT, the results are the means of the family. In addition, in this table, in order to focus on the important data, there is only the maximum of the stress, the Young's modulus (the slope of the elastic part), the maximum value of strain, the σ_{uts}, the $0.2\%\sigma_y$ and the energy. The values are rounded to 10^{-2}, except some value of the maximum of deformation in order to have value.

The mechanical properties of the CPTi are resumed in table 13. However, these values are not from the test but from the literature (Boyer et al., 1996; Institut für Auditierung und Zertifizierung GmbH, 2014) .

Table 12: Table of the means values of the microtension Test

Properties	TNS-1	TNS-2	TNS-3	TNS-4	TNS-5	TNS-7	TNS-8	TNZT
Max stress (MPa)	304.33	74.72	142.73	66.85	316.6	220.43	46.65	424.85
Young's modulus (MPa)	55722	60526	76636.33	19007	92799	41286.4	56071.33	90729.62
Max strain (-)	0.04	0.28	0.01	0.003	0.004	0.15	0.005	0.23
σ_{uts} (MPa)	105.80	23.53	91.00	31.06	57.25	229.94	16.97	331.90
$0.2\%\sigma_y$ (MPa)	101.46	31.84	16. 77	9.60	94.61	220.6	11.32	379.35
Energy ($MPa * m^{0.5}$)	1.45	9.05	0.30	0.13	0.66	36.05	0.34	74.49

Table 13: Table of the mechanical properties of the CPTi grade 3

Properties	CPTi grade 3
Max stress (MPa)	445
Young's modulus (MPa)	105000
Max strain (-)	0.18
$0.2\%\sigma_y$ (MPa)	380

For each member of family of the sample, the typical curve was traced on Excel even if all the values could be obtained through the software Trapezium X. There were also traced on Origin in order to get the σ_{uts} value as in figure 20.

3.4 Correlation

First, in this part it is important to divide the correlation in three parts. The first one is the correlation of the yields stress approximated by the $0.2\%\sigma_y$ with other value such as the P_y^{offest}, P_y^{CWA} and the $Slope^{inti}$. For this correlation the family of sample of the TNS-7 have been united, which means there is only one value for the means of the TNS-7 value. However, as it will be explained later on, this value was far away from the other, and consequently for some correlations, its values have not been taken into account.

The second part is the correlation between σ_{uts} and the $Pmax$ value and the $Slope^{inti}$. For these correlations, the TNS-7 has been divided into two groups as said in part 3.2.1. However, as it will be explained later on, even with this differentiation the values seem still to faraway and have not been always chosen for the correlation.

The third part is the correlation of the energy, the TNS-7 has been divided. However they have not been taken into account.

3.4.1 Correlation of $0.2\%\sigma_y$

First, the correlations between the $0.2\%\sigma_y$ value and the P_y^{offest} and P_y^{CWA} value have been done in figure 30 and figure 31. This correlation takes into account all the value.

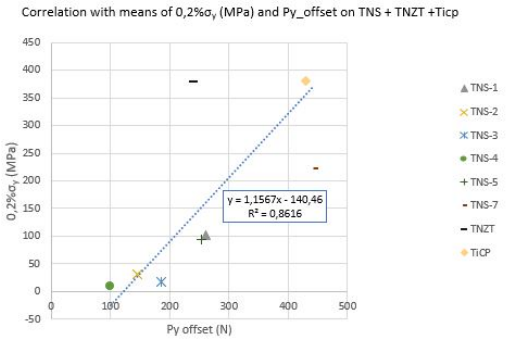

Figure 30: Image of the correlation between means of $0.2\%\sigma_y$ value and means of P_y^{offest} value

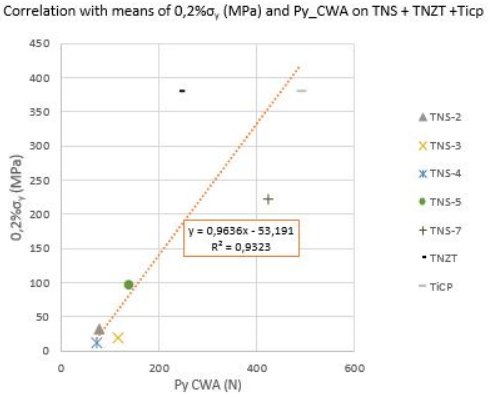

Figure 31: Image of the correlation between means of $0.2\%\sigma_y$ value and means of P_y^{CWA} value

As it was suggested in the literature, the same correlation with P_y^{offest} and P_y^{CWA} divided by the thickness at the order 2 have been made in figure 32 and 33. For this two correlations, only the TNS values have been taken into account. The TNZT and CPTi value were not.

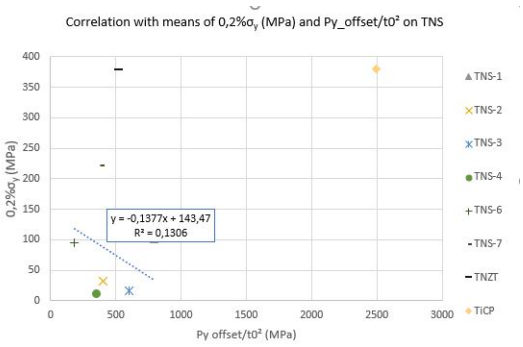

Figure 32: Image of the correlation between means of $0.2\%\sigma_y$ value and means of $P_y^{offest}/t0^2$ value

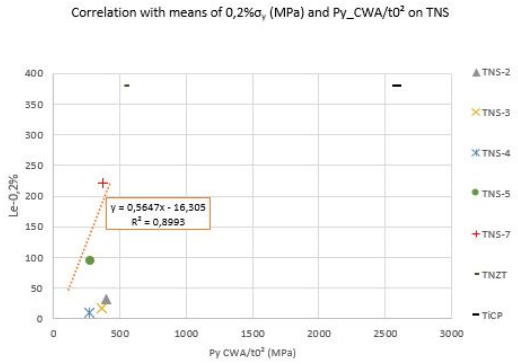

Figure 33: Image of the correlation between means of $0.2\%\sigma_y$ value and means of $P_y^{CWA}/t0^2$ value

The correlation with the P_y^{offest} and P_y^{CWA} divided by the thickness have been made in figure

34 and 35. In order to have better correlation, the TNS-7 values have not been taken into account.

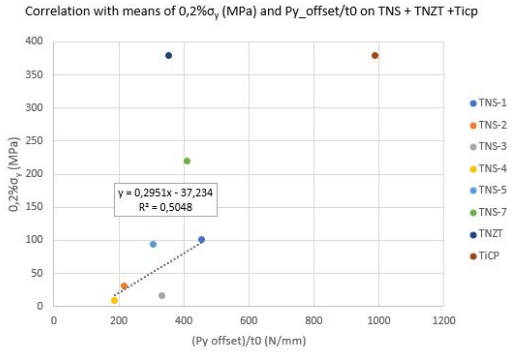

Figure 34: Image of the correlation between means of $0.2\%\sigma_y$ value and means of $P_y^{offest}/t0$ value

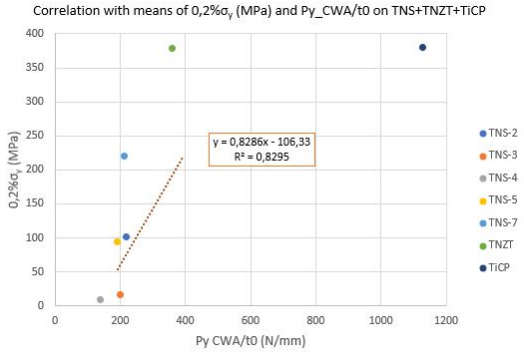

Figure 35: Image of the correlation between means of $0.2\%\sigma_y$ value and means of $P_y^{CWA}/t0$ value

The correlation with the P_y^{offest} and P_y^{CWA} divided by the multiplication of t0 by Zm are represented in figure 36 and 37. In order to have a better correlation factor (R^2), on the first correlation only the TNS was used while for the second only the TNZT was not used.

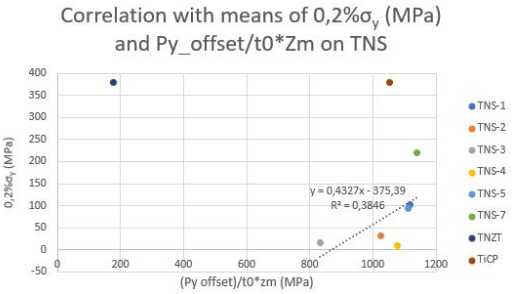

Figure 36: Image of the correlation between means of $0.2\%\sigma_y$ value and means of $P_y^{offest}/t0 * Zm$ value

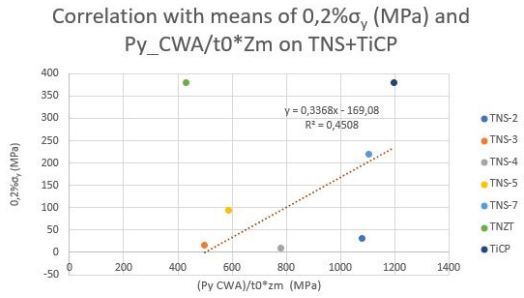

Figure 37: Image of the correlation between $0.2\%\sigma_y$ value and the $P_y^{CWA}/t0 * Zm$ value

Finally, the correlation with the $Slope^{inti}$ divided by the thickness as it is suggested in part 1.1.2.v is shown in figure 38. The TNS-7 values have not been taken into account in order to increase the correlation factor.

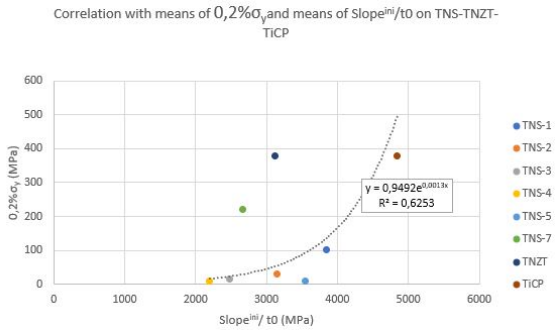

Figure 38: Image of the correlation between means of $0.2\%\sigma_y$ value and means of $Slope^{inti}/t0$ value

3.4.2 Correlation of σ_{uts}

For this correlation, the methodology made from the other authors have been followed. The correlation with $Pmax$, then with $Pmax/t0$, $Pmax/t0^2$ and finally with $Pmax/(t0{*}Zm)$. The correlations with the $Slope^{inti}/t0$ have also been made. All these correlation are in the respective figure 39, 40, 41, 42 and 43. For all these correlation the TNS-7 values have been divided into two groups as said previously. For the correlation between σ_{uts} value and the $Pmax/t0$ value, and the correlation between σ_{uts} value and the $Slope^{inti}/t0$ value, the TNS-7.1 and TNS-7.2 have not been taken into account.

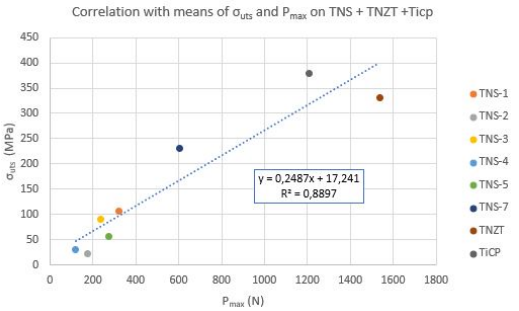

Figure 39: Image of the correlation between means of σ_{uts} value and means of $Pmax$ value

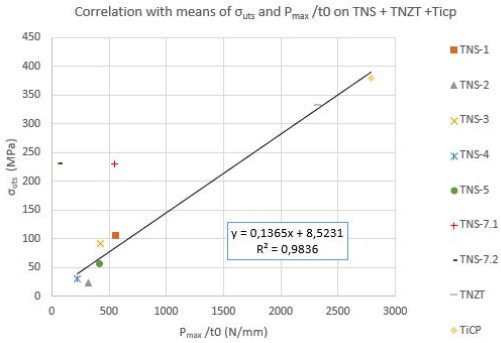

Figure 40: Image of the correlation between means of σ_{uts} value and means of $Pmax/t0$ value

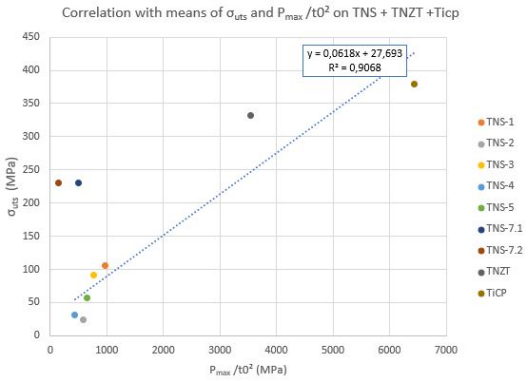

Figure 41: Image of the correlation between means ofσ_{uts} value and means of $Pmax/t0^2$ value

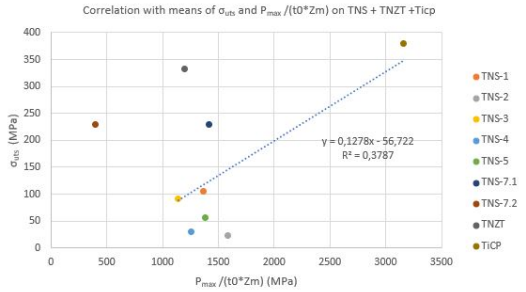

Figure 42: Image of the correlation between means of σ_{uts} value and means of $Pmax/(t0 * Zm)$ value

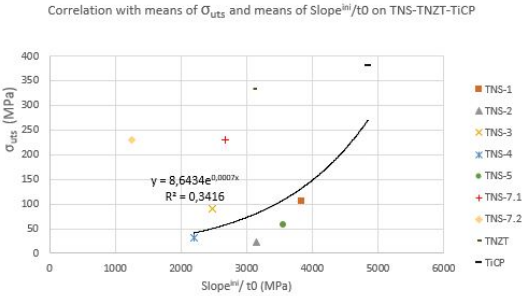

Figure 43: Image of the correlation between means of σ_{uts} value and means of $Slope^{inti}/t0$ value

3.4.3 Correlation of the Energy

The last correlation made was between the energy of the two tests. As the CPTi has not been tested with the microtension Test, the CPTi value has not been taken into account. The figure 44 shows this correlation.

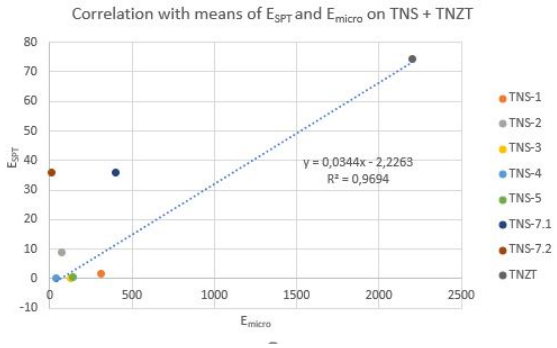

Figure 44: Image of the correlation between the means of energy of the probes

4 Discussion

In this part, the discussion of the results given previously will be done. Following the same pattern as the pattern of the results the discussion of the phase in presence of the different alloy will be done.

Afterwards, the analyse and discussion of the results given by the SPT and the microtension test will be the second part.

The third part will focus on the analyse and discussion of the correlation factor available at the end of the result part.

4.1 Analyse of the phases

The titanium is known to have 2 different allotropic forms. The first one the α phase which is a hexagonal close-packed (**HCP**) structure. The second one which is the β phase, a centered cubic (**CC**) crystal structure.

The niobium and tantalum are known to be β-isomorphic stabiliser while the zirconium and the tin are neutral (Amigó Borrás, Curso 2019-2020).

As said previously, some TNS alloy have been made with (3%wt) of magnesium. However, the alloy made with magnesium have the same number of pics and the same pic. The only difference is the intensity of the third pic (the $\beta - (101)$) which seem higher for the TNS made without magnesium.

It is not surprising to have the presence of the α and β phase for all the probes due to the fact that niobium is a β-isomorphic stabiliser. However, the intensity and consequently the amount in percentage of β phase is for all the sample higher and are in majority. This enables to say that the TNS alloy made by this sintering process after a milling time of 72h generate a β-phase titanium alloy. Nevertheless, it is important to do not forget that the niobium has a mesh parameter next to

the one of the β phase of the titanium, and consequently can interfere on the results. In addition, in this laboratory, the same alloys through another technique of sintering (Electronic Resistance Sintering) have been studied. Their XRD analysis were quite similar as the ones obtained in part results.

The TNZT sample is, as the TNS samples, an alpha and beta phase titanium alloy. The β phase is present in majority while the α is not. In the literature the TNZT is known to have microstructure including a matrix of β phase (CC) with α phase grain boundary precipitates (Niinomi, 1998; Rechtin et al., 2018). Even if the phases are directly dependent of the process used to create the material, the presence and majority of β phase seems coherent.

In conclusion, for the phases, there is two beta (bcc structured) alloy the TNS and TNZT and one alpha (hexagonal compact) for the CPTi.

The fact to add magnesium does not change the amount of phase for the TNS but the size of the pics. In addition, the TNS and the TNZT are quite similar. However, some crystalline plans are present in the TNS and not in the TNZT and vice-versa. The difference between the two graphs is the presence of the α plan (201), (112), (102) and (101) β plan for the TNS and the presence of the α plan (103) for the TNZT.

4.2 Analyse of the results of the two tests

Now, this part of the report will focus on the results obtained through the two mechanical tests.

4.2.1 The Small Punch Test

First, it is important to remind that it was the first use of the Small Punch Test device in this laboratory. The curve obtain seems for the majority of them to correspond of the curve that it is possible to obtain through this kind of test as it is possible to see on the part 1.1.2.iv of this report.

Before any discussion of the results, a short aside of the thickness of the samples of SPT needs to be done. Indeed, in this research the thickness of the probes of TNS was not controlled as much as it could have been done, and as much it has been done in some others researches. In fact, in this research, the probes thickness desired was $\approx 0.5mm$, however the mean of all the probes is 0.6 mm of thickness and variate between 0.427 and 1.199 mm. In other research such as in the paper of Janca et al., 2016, it did not exceed $\pm 0.5\mu m$. In a less accurate research made by García et al., 2013 the variation is about 0.1 mm, however this variation is lower than for the TNS probes. On the other hand, the thickness of the CPTi samples and TNZT samples the variation have been more controlled ($\pm 0.1mm$ for the CPTi and $\pm 0.2mm$ for the TNZT). This has consequently led to huge variation in results for the TNS, it is possible to see it especially with the TNS-7 family, and that is why this family have been divided into two groups by size as explained before.

The mechanical behaviour of the samples could be divided into two groups, the CPTi and TNZT which are ductile, and the TNS which is less ductile than the 2 first one, and it could almost be consider as a semi-brittle material. Between the two ductile materials, the TNZT is by its means more ductile (energy of fracture, $Pmax$, Zm, higher than the ones of CPTi). For the CPTi and for the TNZT the $Pmax$ value is far away from the P_y^{offset} and from the P_Y^{CWA} this is probably linked with the fact that they have a more important zone of plasticity and consequently are more ductile than the TNS. In addition, the range of value of the P_y^{offset} and the P_Y^{CWA} are at the same order of magnitude (hundreds of newton) than others materials found in the paper of García et al., 2013.

There are few papers on the SPT of the titanium alloys, however some of the commercial titanium have been studied. The first one, the more famous, the Ti-6Al-4V (titanium grade 5) (Roger Hurst, 2016) and the second one titanium grade 2, TA2 (Lin Xue, 2019). Thanks to these two tests, it is possible to see that the $Pmax$ value from this two alloys are respectively $Pmax =\sim 1500N$ and $Pmax$ value of the Ti-6Al-4V $= [1200 - 1400]N$ depending of its fabrication. Consequently the mean found on the CPTi grade 3 seems logical or at least next to the true value.

From the photography of the SPT sample after the test it is possible to see a huge difference between the fracture. The one of the CPTi has cracks more circular and concentric while the ones of the TNS sample are more radial and brutal. This is a sign of the difference of the ductility of the two alloys. A more circular and concentric fracture is a sign of the ductility of the material while the radial cracks is a sign of a more brittle material this is confirm by the thesis made by Avila, 2019.

4.2.2 The Microtension test

From the results given in table 12 the first thing which is remarkable is the really low values of the TNS sample and their brittle comportment. In addition the TNS-2, TNS-4 and TNS-8 values are really low (Max stress lower than the hundred of MPa). The article made by Peiyou Li1, 2019 gives values of a comparable alloy of with different chemical composition of TNS. The closest one of the alloy made in this research is the $Ti_{75}Nb_{20}Sn_5$. Its mechanical properties are given and are $0.2\%\sigma_y = 435MPa$. In order to have another value to compare it, the Ti-25Nb has $0.2\%\sigma_y = 872.5MPa$ (Yuqing Zhang, 2020). From theses two articles, it is possible to suggest that the value obtain from the microtension test are abnormally low.

Even if the value of the TNZT are much higher, and in the good order of magnitude, the accuracy of the result is to discuss. Indeed the article made by Niinomi, 1998 gives the mechanical values of the $\sigma_{uts} = 596.7MPa$ and $0.2\%\sigma_y = 547.1MPa$, which is respectively ~ 1.8 times and ~ 1.44 times higher than the values of this research.

The difference between the results could be from the difference compactness of the materials or their sintering process or sintering parameters. Another likely possibility of the huge variation

between theses results and the one of the literature is the use of a microtension test and not a bulk size test. However, as the work is done on stress and not on force, the values should not have been so far from the bulk size test. In addition the article made by Terumitsu Miura, 2018 confirms the fact that the value of a microtension test is commonly close to the value of a bulk size test.

Last but not least, as explain previously, the value of the σ_{uts} was hard to determine in this research and their accuracy may be not the best, this is also a possibility of mistake.

However, the value of the Young's Modulus is the good order of magnitude and really close to the literature value such as the one of Peiyou Li1, 2019 ($\sim$ 60GPa for the TNS in the literature against $\sim$ 57 GPa in this reasearch) . The Young's Modulus of the TNZT is known to be 55 GPa and much lower than the commercial titanium (Niinomi, 1998). Here, even if the value is lower than the value of the commercial titanium it is $\sim$1.6 times higher.

From the stress-strain graph present in the appendixe B, it is possible to note the fact that the TNS are brittle (non presence of an plastic zone). The TNZT on the other hand has a huge elastic zone, and consequently present a ductile comportment.

4.3 Discussion of the correlation factors

In this part, the discussion of the correlation factor will be done. First, an overview of the factor obtained between the different correlation, and their the correlated factor will be done.

In a second part, the factor found will be compared to the factor that exist already in the literature.

It is really important to take into account the previous discussion made on the results of the SPT and of the microtension test as the correlation have been made by using theses results.

4.3.1 Correlation of $0.2\%\sigma_y$

In this part the discussion of the different correlation of the $0.2\%\sigma_y$ value will be done, and compared of the one pre-existing in the literature.

Table 14: Resume of the R^2 value of $0.2\%\sigma_y$

	P_y^{offset}	P_Y^{CWA}	$P_y^{offset}/t0$	$P_Y^{CWA}/t0$	$P_y^{offset}/t0^2$	$P_Y^{CWA}/t0^2$	$P_y^{offset}/t0 * Zm$	$P_Y^{CWA}/t0 * Zm$
R^2 value	0.8616	0.9323	0.5048	0.8295	0.1306	0.8993	0.3846	0.4508

In the table 14 all the R^2 values are resumed. Firstly, the P_Y^{CWA} has always a better correlation than the P_y^{offset} especially when the order of the thickness of the denominator increase. In addition the two values when the division is made by the maximum of displacement times the thickness are too low and cannot be considered as good correlation.

The correlation with P_Y^{CWA}

The P_Y^{CWA} has good correlation even if in the literature, better correlate factor have been found (up to 0.99) as in the article made by Jose Calaf Chica, 2018, by García et al., 2013 and by Janca et al., 2016. In addition, while dividing by the thickness at the second order the correlated factor seems not affected a lot whereas it should.

As observed in the literature, the value α_1 variate between 0.08 and 0.51. The values obtained seem consequently higher than usual (respectively 0.96, 0.83, 0.56, 0.34). In conclusion, the correlation with the better R^2 and a good α_1 range of value is the correlation with the $P_Y^{CWA}/t0^2$ as it is suggested in the literature.

The correlation with P_y^{offset}

The method of determination of this offset method is different as the one it is possible to find in the literature. This method, as explain before, is the intersection between the force-displacement curve and the parallel of the slope of the region I. In order to have a point to be able to trace this second curve, the value of x corresponds to a relative elongation $\epsilon = 0.2\%$. Even if this method is different from the one in the literature it is really similar at the one explained in part 1.1.2.iv.

However, except from the first correlation without normalising the P_y^{offset}, none of the correlations have correlated factor enough high. In addition, the α_1 range of value is far away from the one found in literature such as in the paper of Jose Calaf Chica, 2018, or García et al., 2013, and Janca et al., 2016.

Consequently, these correlation are not able to work in this case, however, the idea of using this P_y^{offset} is not to throw away and be maybe in some case comparable to the more famous one when the aim is not using the relative elongation but a percentage of the initial thickness.

Finally, the correlation with the $Slope^{inti}/t0$ as a $R^2 = 0.63$, far from the 0.997 found in literature (Jose Calaf Chica, 2018). However, with more accurate results and with more results the correlation could be better. The idea of correlating with the $Slope^{inti}/t0$ is to be pursued.

4.3.2 Correlation of σ_{uts}

The table 15 resumes the R^2 of the correlation with σ_{uts}. Except from the $Pmax/(t0 * Zm)$ all the R^2 are acceptable $R^2 \approx 0.9$ or higher.

Table 15: Resume of the R^2 value of σ_{uts}

	$Pmax$	$Pmax/t0$	$Pmax/to^2$	$Pmax/(t0 * Zm)$
R^2 value	0.89	0.98	0.90	0.38

The division by $(t0 * Zm)$ is as much as the one for the P_y correlation not acceptable. The value of the correlated factor is far way from the one possible to find in literature. This is maybe due to

the determination of the Zm or of the size of the probes. As the probes were not all with the same thickness nor with the same diameter, the Zm value could have been dependant of this.

Nevertheless, good correlation with the $Pmax$ value have been found. In addition, not only the values of the correlated factor are sufficient but the value of β_1' and β_1 respectively 0.14 and 0.06 are in the same range of order as the one found in literature as said previously $[0.08 : 0.51]$. It is important to note that better correlation by dividing only by the order one of the thickness have been found than by the order 2. This permits to explain the presence of the correlation by dividing only by the thickness even if the units are not the same for the correlation. In order to compare with the literature, better correlation factor have been found than in the article of García et al., 2013 (only $R^2 \approx 0.4$).

The correlation with $Slope^{inti}/t0$

The R^2 value is 0.34 for this correlation. However, it was the first time (or at least present in the results part of the literature) that this correlation have been made. Indeed, the correlation with the slope was made with the yield stress and not the ultimate tensile stress. The lack of information to compare is maybe due to the fact that authors have not decided to present this results with maybe a bad correlation. It is also possible that this correlation is not interesting. However, it was though that present this correlation in order to compare it with the correlation with the yield stress is interesting and show that the correlation with the yield stress is better and need may be more focus in term of research.

4.3.3 Correlation of the energy

The energy of the sample of the two test seems well correlated, $R^2 = 0.9694$. It is important to note that the energy calculated was the area under the curve. As the two curves do not have the same ordinate axis the energy was not calculated from the same base and unity.

Indeed, fracture toughness in the case of a stress-strain curve is expressed in units of stress times the square root of crack length, that is, $MPa * m^{0.5}$. In the case of the force-displacement it is express by force times the square root of crack length times the displacement $N * m^{1.5}$.

A remarkable point of this correlation is the fact that it takes into account the micro-size of the tests. As the two tests are working at the micro-size, the energy calculated was on micro-size probes and consequently their size was already take into account.

This point is important, indeed some previous correlations on the energy were made but not conclusive due to the fact that the energy from the SPT (micro-size) was compared to energy from bluk size traction or Charpy test which is also a macro-size test.

It is also important to note that is one of the first time that the correlation of the energy of these two tests have been made, and consequently cannot be compare to others test.

4.4 Conclusion of the discussion

In conclusion of the results, the alloy with a majority of α phase is the CPTi. The two others alloys have the β phase in majority and have almost the same plan. In addition adding the magnesium to the TNS alloy has not change its phases, a small augmentation of the intensity of the plan β -(101) have been noticed.

In addition, the results obtain from the SPT seem the more accurate between the two tests and have the results more close to the one that it is possible to find in literature. Notwithstanding, the two tests have enabled to see the mechanical behaviour of the different alloys and their types of fracture.

In addition, the some good correlations (especially between σ_{uts} and $Pmax$ and its respective normalisation) have been made despite the fact the results seem not totally accurate.

5 Conclusion

This report resumed 4 months of investigation on the validation of the mechanical properties of sintered material through the use of microprobes.

A first part of the states of the art explaining the previous knowledge of this subject and focusing especially on the SPT shows the knowledge obtained thanks to the literature.

The motivation, justification and objective of the research enables to understand the meaning and the aim of this research.

Then a part explaining the methodology followed during all the investigation enables the reader to do it by itself and consequently verify the results. This part also enables to explain some decision taken during theses 4 months.

Then following a paper methodology report the materials have been presented. The materials have been sintered and tested. The CPTi, the TNS (with and without magnesium) and finally the TNZT. Three alloys of titanium in order to have a base of comparison. First a XRD analysis has been done on the sample in order to see their phases in presence. Then two mechanical tests, the first one the SPT, first used in this laboratory for this research and then the microtensile test already known by this laboratory.

Last but not least, the correlations following the methodology used in different papers previously cited have been done in order to increase the amount of correlation between SPT and microtensile test. Some correlations discussed previously have been found and could, for some, be used.

6 Futur work

In this part a little discussion of the future work that could be done on this research will be done.

First, as the results obtain from the microtension test are not totally satisfactory, it could be interesting to do some others in order to maybe reduce the difference with the previous research made by some authors.

Secondly, as it has been done in many papers previously cited a numerical analysis through the finite element could be done in order to see if the results obtained are coherent with the numerical results. This could also enable to see if the breaking of the probes follow the predictions made by the numerical calculus and consequently if the SPT and the microtensile test have been made correctly.

A third point of investigation could have been the correction of the energy with a bulk size test such as the Charpy test. Indeed, in order to see if the energy generated by the rupture of the probe through SPT or microtensile test could be linked to the energy of the breaking through a Charpy test, this test could have been done and the correlation following the same methodology as used in this report or in all the papers cited could have been done too.

References

Albakry, M., Guazzato, M., & Swain, M. V. (2003). Biaxial flexural strength, elastic moduli, and x-ray diffraction characterization of three pressable all-ceramic materials. *The journal of prosthetic density*, *89*.

Al-Rub, R. K. A. (2007). Interfacial gradient plasticity governs scale-dependent yield strength and strain hardening rates in micro/nano structured metals. *International Journal of Plasticity*, *24*.

Avila, D. S. (2019). *Análisis y mejora de la caracterización mecánica mediante ensayos miniturizadoq de aleaciones procesadas por fabricación aditiva*.

Borrás, V. A. (Curso 2019-2020). Módulo 2 biometales unidad 2.3 aleaciones de titanio.

Boyer, R., Welsch, G., & Collings, E. W. (1996). *Materials properties handbook: Titanium alloys edition john m. (tim) holt technical ed.* http://asm.matweb.com/search/SpecificMaterial.asp?bassnum=MTU030 (accessed: 16.11.2020)

CHERFAOUI, M. (2006). Essais non destructifs. Editions T.I.

Duncombe, E. (1972). Plastic instability and growth of grooves and patches in plates or tubes. *International Journal of Mechanical Sciences*, *14*. https://doi.org/https://doi.org/10.1016/0020-7403(72)90087-2.

Éric Badel, P. P. (1999). Détermination des propriétés élastiques d'élémentsindividuels du plan ligneux du chêne par des essaisde traction sur micro-éprouvettes. *Ann. For. Sci.*, *56*, 467–478.

García, T., Rodríguez, C., Belzunce, F., & Suárez, C. (2013). Estimation of the mechanical properties of metallic materials by means of the small punch test. *Journal of Alloys and Compounds*, *582*, 708–717.

George Z. Voyiadjis, M. Y. (2019). Chapter 1 - introduction: Size effects in materials. https://doi.org/https://doi.org/10.1016/B978-0-12-812236-5.00001-3.

Gudlavalleti, S. (2002). Mechanical testing of solid materials at the micro-scale. https://core.ac.uk/download/pdf/4396927.pdf

Hosford, W. F., & Caddell, R. M. (2011). Plastic instability. *Metal forming: Mechanics and metallurgy* (4th ed., pp. 43–51). Cambridge University Press. https://doi.org/10.1017/CBO9780511976940.005

J. Ruud, A. L. G., D. Josell, & Spaepen., F. (1992). The elastic moduli of silver thin films measured with a new microtensile tester. *MRS Symposium Proceedings*, *239*, 239–243.

Janca, A., Siegl, J., & Hausild, P. (2016). Small punch test evaluation methods for material characterisation. *Journal of Nuclear Materials*.

Jose Calaf Chica, M. P. C., Pedro Miguel Bravo Díez. (2018). Development of an improved prediction method for the yield strength of steel alloys in the small punch test. *Materials Design*, *148*. https://doi.org/https://doi.org/10.1016/j.matdes.2018.03.064.

Lin Xue, S. Y., Xiang Ling. (2019). Mechanical behaviour and strain rate sensitivity analysis of ta2 by the small, punch test. *Theoretical and Applied Fracture Mechanics*, 9–17.

Manahan, M. P. (1983). A new postirradiation mechanical behaviortest—the miniaturized disk bend test. *Nuclear Technology*, *63*. https://doi.org/10.13182/NT83-A33289

MAO, X., & TAKAHASHI, H. (1987). Development of a further-miniaturized specimen of 3 mm diameter for tjzm disk (0 3 mm) small punch test. *Journal of Nuclear Materials*, *150*, 45–52.

Morrell, R. (Review in 2007). Biaxial flexural strength testing of ceramic material. National Physical Laboratory.

national Members, C. (2007). Small punch test method for metallic materials.

Niinomi, M. (1998). Mechanical properties of biomedical titanium alloys. *Materials Science and Engineering: A*, *243*, 231–236. https://doi.org/https://doi.org/10.1016/S0921-5093(97)00806-X.

Peiyou Li1, D. W. H. Z., Xindi Ma. (2019). Microstructural and mechanical properties of-typeti–nb–sn biomedical alloys with lowelastic modulus. *MDPI Journal*.

Read., D. T. (1998). Tension-tension fatigue of copper thin films. *International Journal of FatigueInternational Journal of Fatigue*, *3*, 203–209.

Rechtin, J., Torresani, E., Ivanov, E., & Olevsky, E. (2018). Fabrication of titanium-niobium-zirconium-tantalium alloy (tnzt) bioimplant components with controllable porosity by spark plasma sintering. *Materials*, *11*, 181. https://doi.org/10.3390/ma11020181

Roger Hurst, S. J., Robert Lancaster. (2016). The contribution of small punch testing towards the development of materials for aero-engine applications. *Theoretical and Applied Fracture Mechanics*, 69–77.

Simonovski, I., Holmström, S., Baraldi, D., & Delville, R. (2020). Investigation of cracking in small punch test for semi-brittle materials. *Theoreticaland AppliedFracture Mechanics*, *108*.

Simonovski, I., Holmström, S., & Bruchhausen, M. (2016). Small punch tensile testing of curved specimens:finite element analysis and experiment. *International Journal of Mechanical Sciences*. https://doi.org/http://dx.doi.org/10.1016/j.ijmecsci.2016.11.029

Terumitsu Miura, K. F. (2018). Micro-tensile testing of reduced-activation ferritic steel f82h irradiated with fe and he ions, *Nuclear Materials and Energy*, 24–28. https://doi.org/https://doi.org/10.1016/j.nme.2018.08.004.

TODUA, P. A. (2005). Metrology and standardization in nanotechnologies and the nanoindustry meas. *unknown*, *51*(5), 462–469. https://doi.org/http://elsvier.com

Vautrot, M. (n.d.). *Etude du comportement mécanique des matériaux dans des conditions étendues de vitesses et de températures: Application à l'acier c68 dans le cas d'une opération de formage incrémental*. https://tel.archives-ouvertes.fr/tel-00795973/document (accessed: 06.11.2020)

W. N. Sharpe, B. Y., & Edwards., R. L. (1997). A new technique for measuring the mechanical properties of thin films. *Journal of Microelectro mechanical Systems*, *6*, 193–198.

Wen, Cheng, Tong, X., Gua, & Kaishu. (2016). Correlation factor study of small punch creep test and its life prediction. *Materials*, *9*. https://doi.org/10.3390/ma9100796

Yang, Z., & Wang, Z.-w. (2003). Relationship between strain and central deflection in small punch creep specimens. *International Journal of Pressure Vessels and Piping*, *80*.

Yuqing Zhang, J. C., Danni Sun. (2020). Techanical and biological properties ofti–(0–25 wt)nb alloys for biomedical implants application. *Regenerative Biomaterials*. https://doi.org/10.1093/rb/rbz042

appendixes

Appendix A Dimension of the SPT device

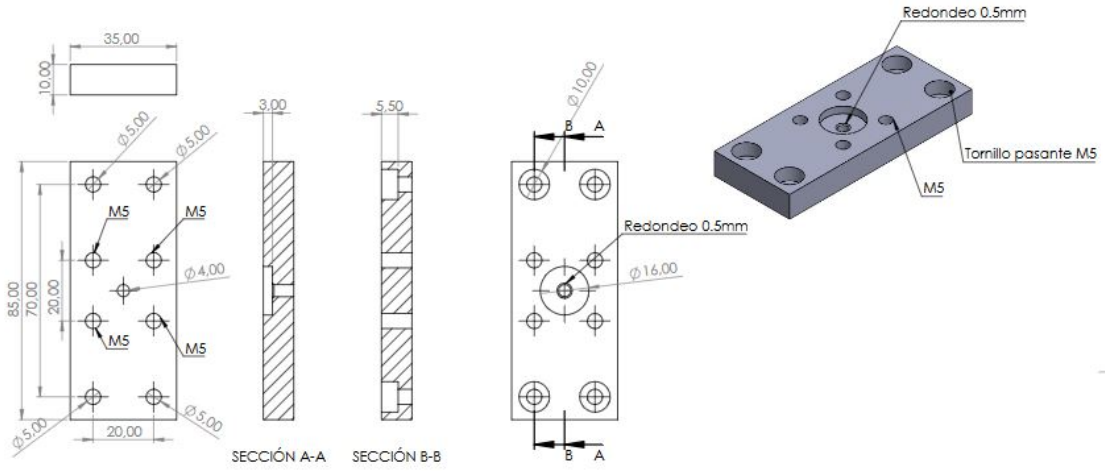

Figure 45: Plan of the base of the SPT device

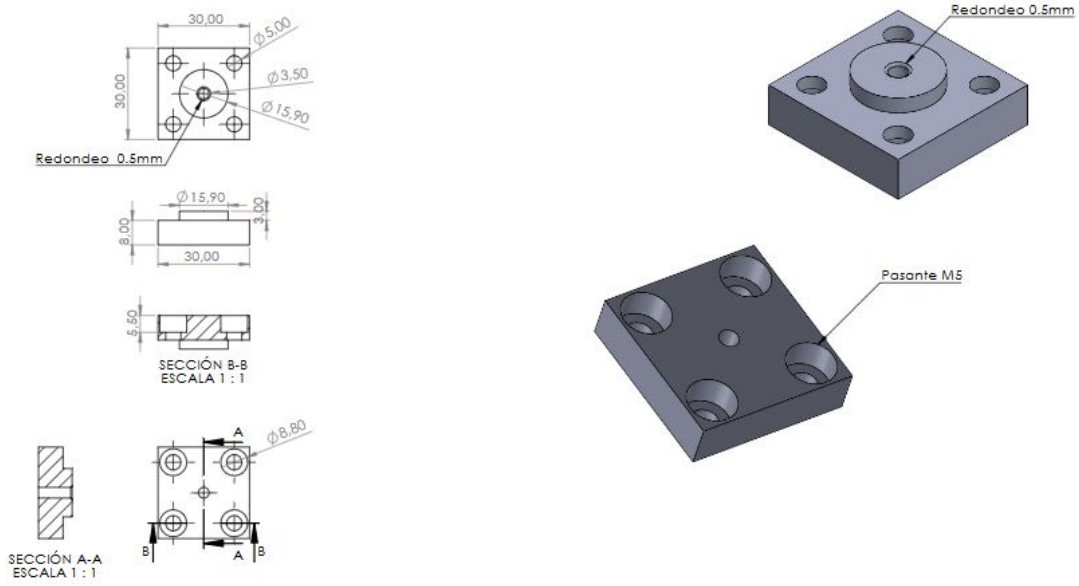

Figure 46: Plan of the upper part of the SPT device

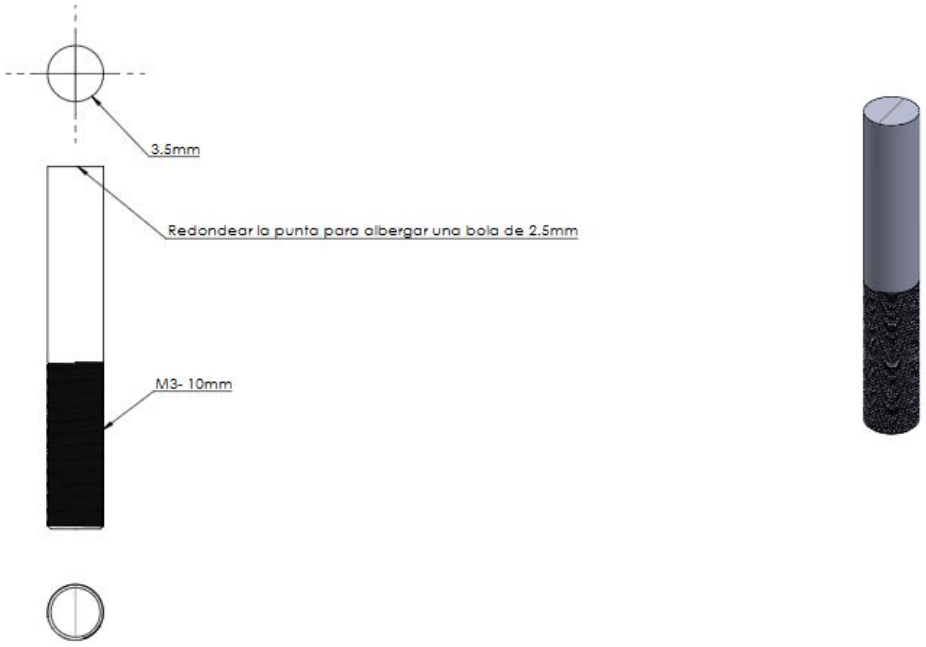

Figure 47: Plan of the tip of the SPT device

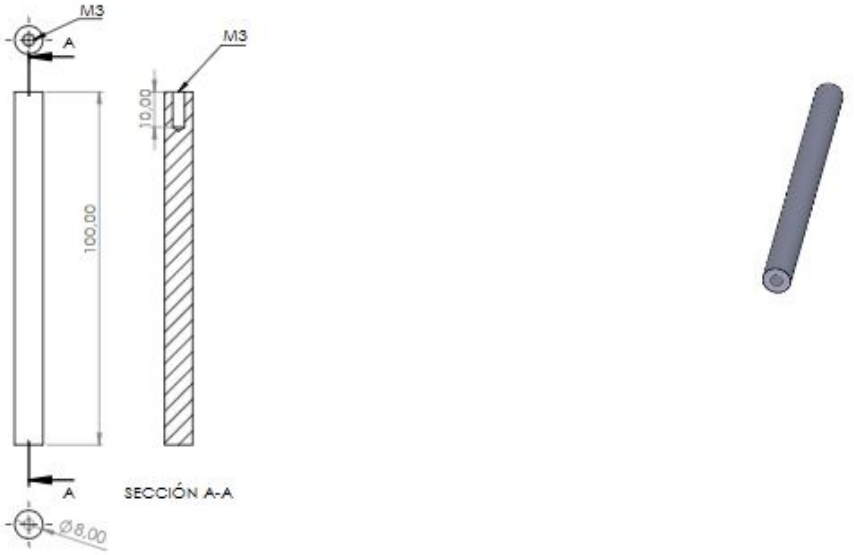

Figure 48: Plan of the punch of the SPT device

Appendix B Results

B.1 Results of SPT

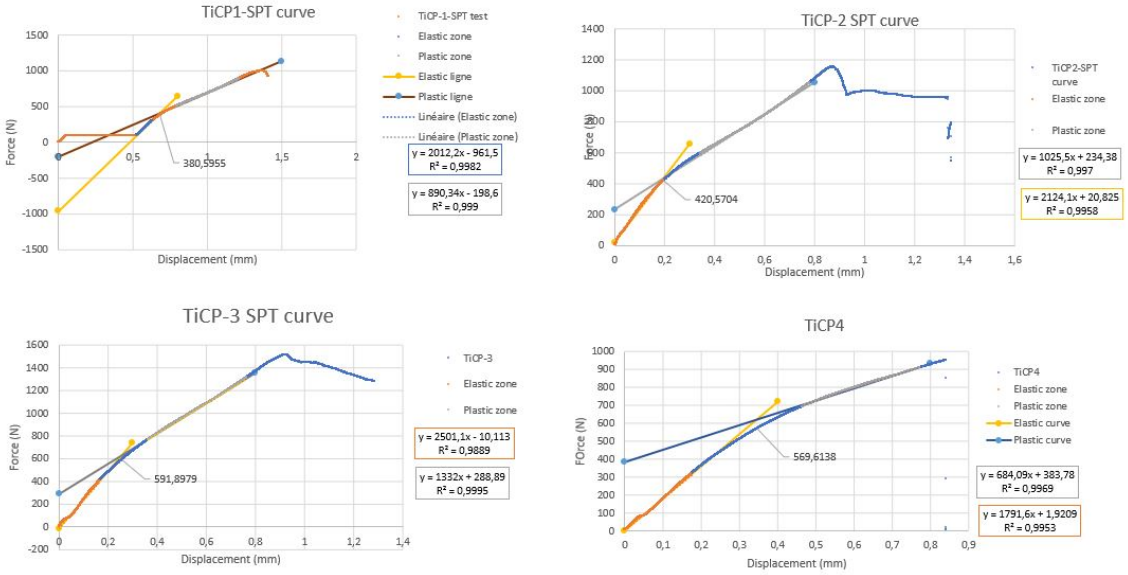

Figure 49: SPT curve of the CPTi

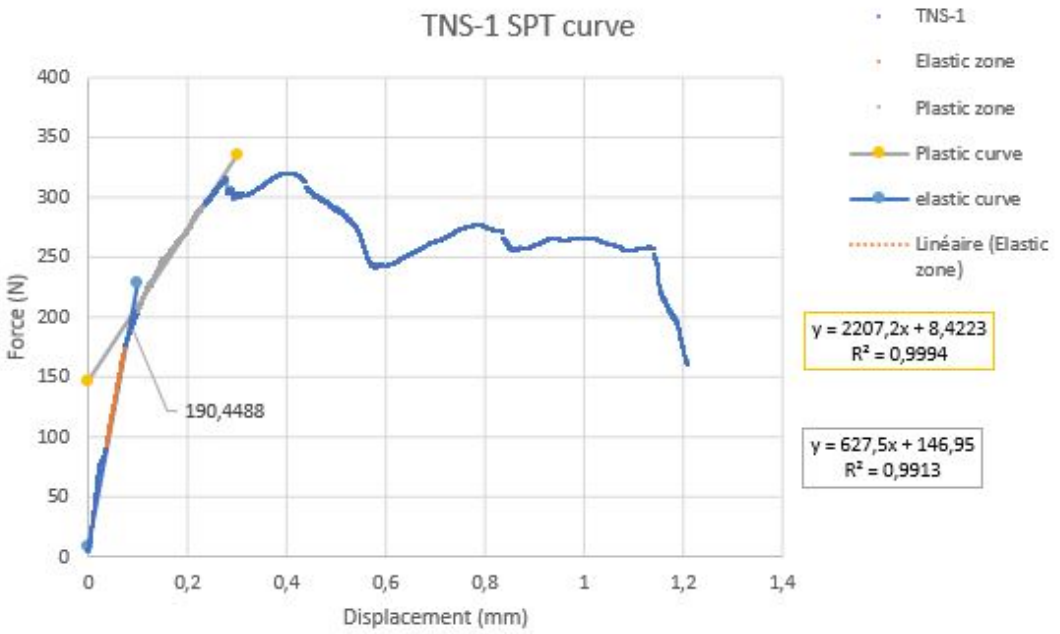

Figure 50: SPT curve of the TNS-1

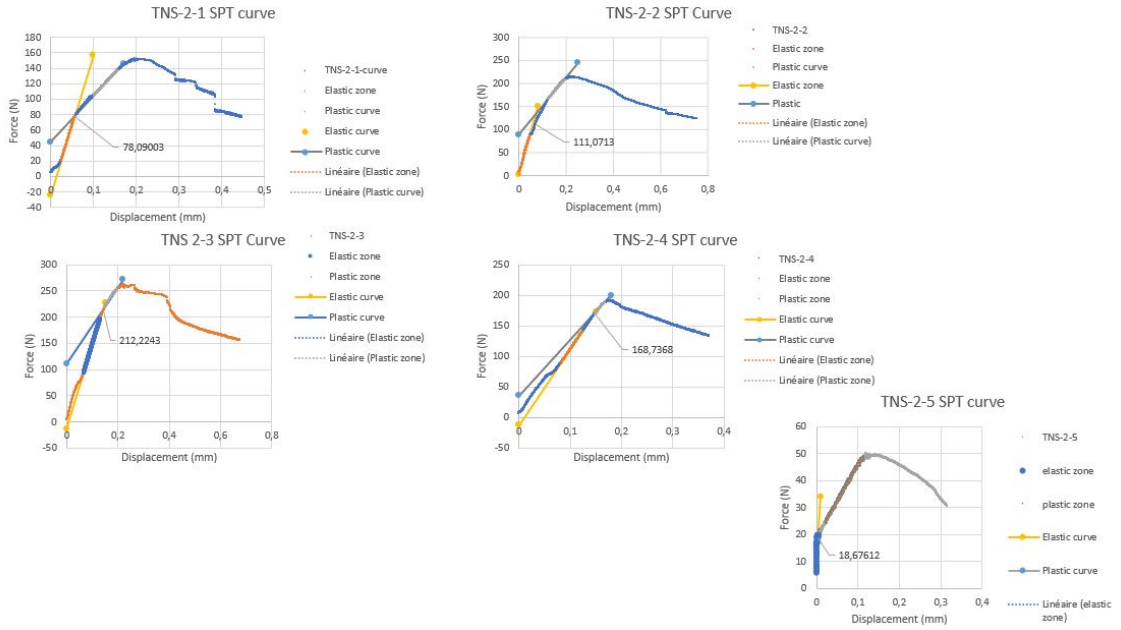

Figure 51: SPT curve of the TNS-2

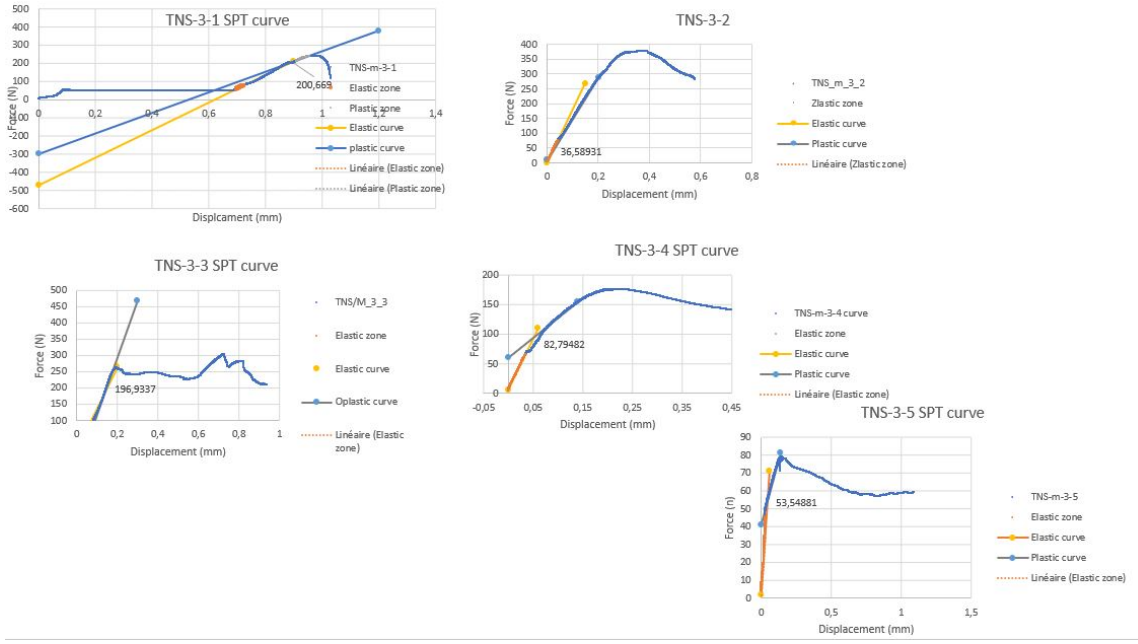

Figure 52: SPT curve of the TNS-3

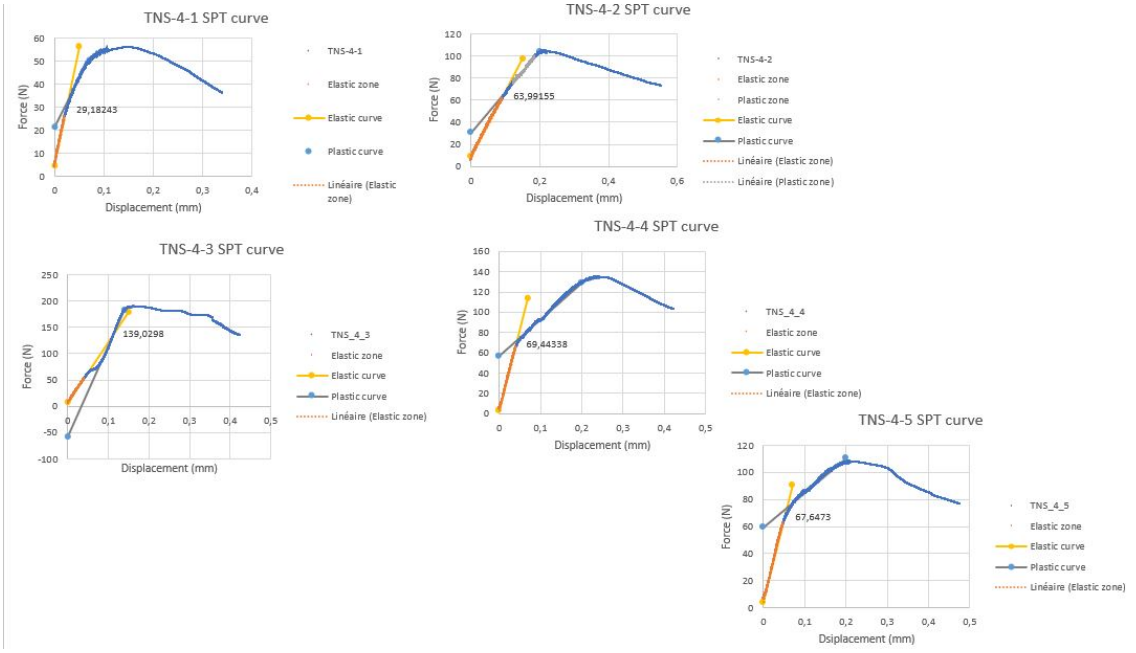

Figure 53: SPT curve of the TNS-4

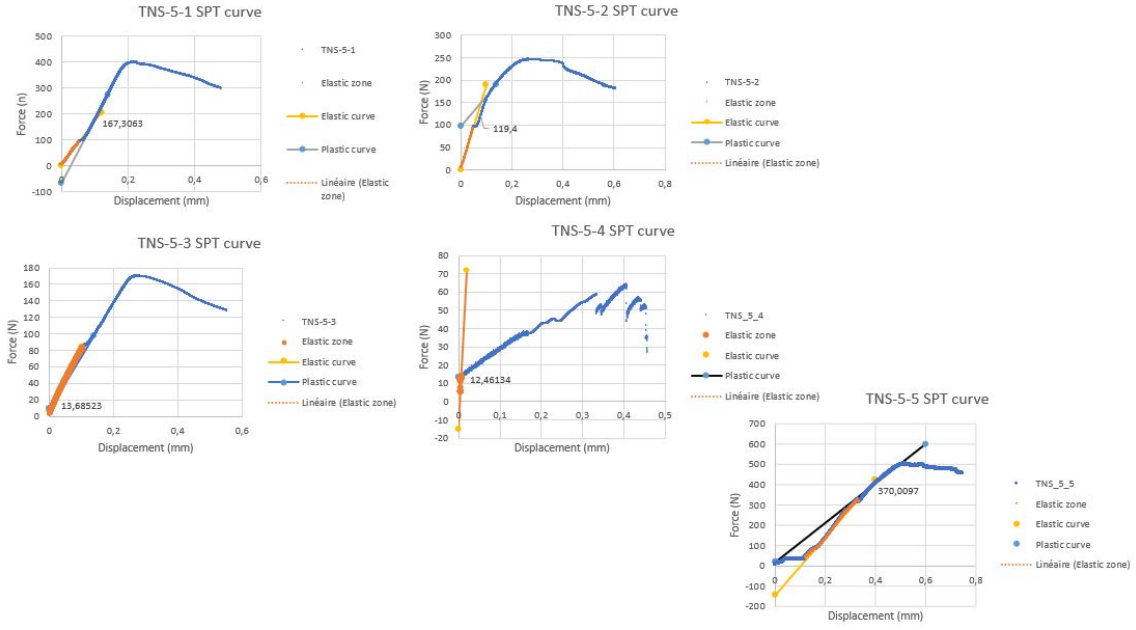

Figure 54: SPT curve of the TNS-5

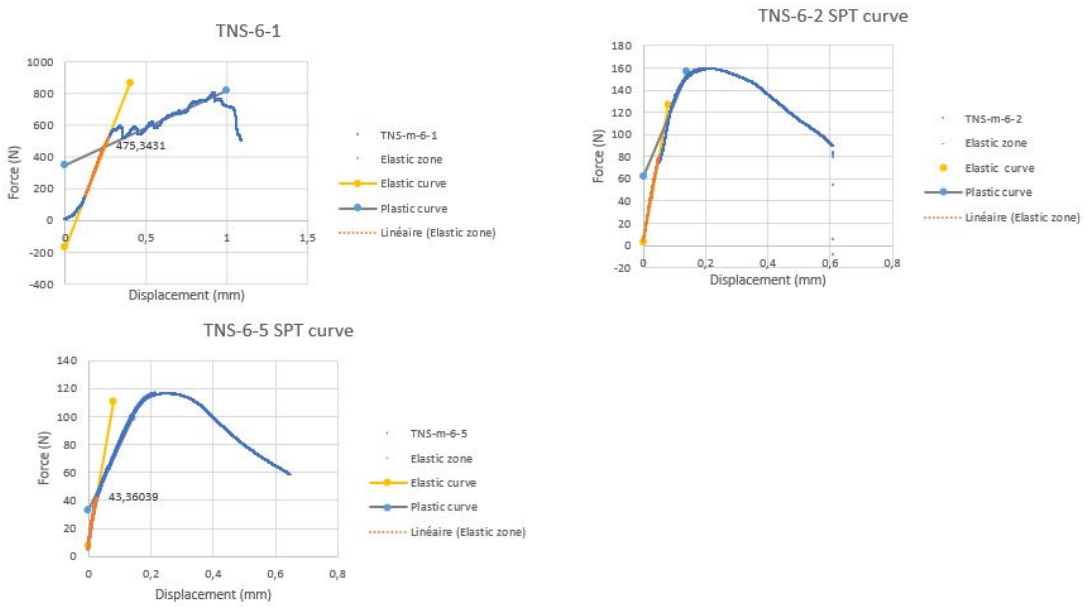

Figure 55: SPT curve of the TNS-6

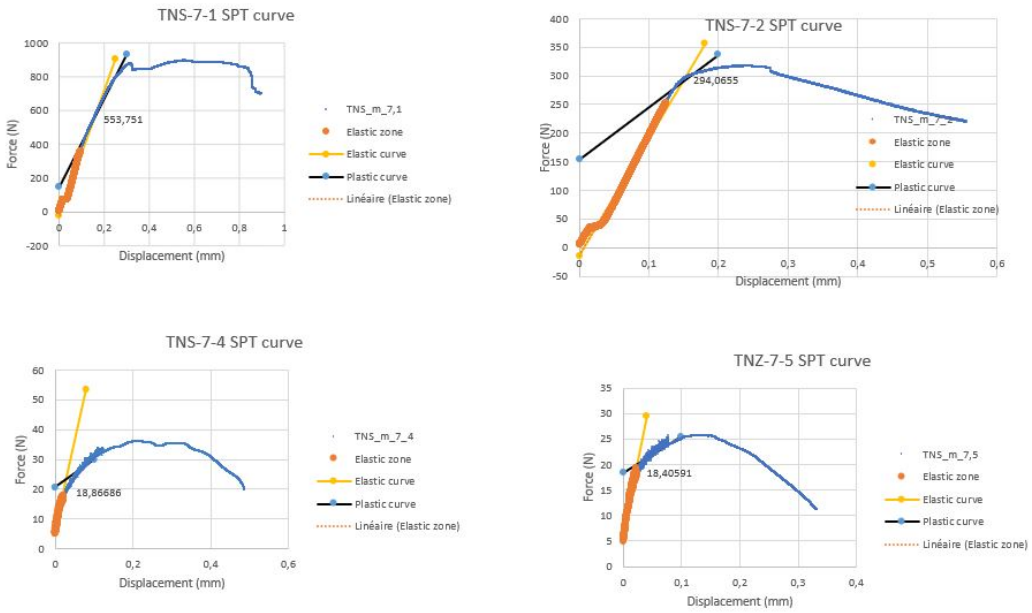

Figure 56: SPT curve of the TNS-7

B.2 Observation by microscope

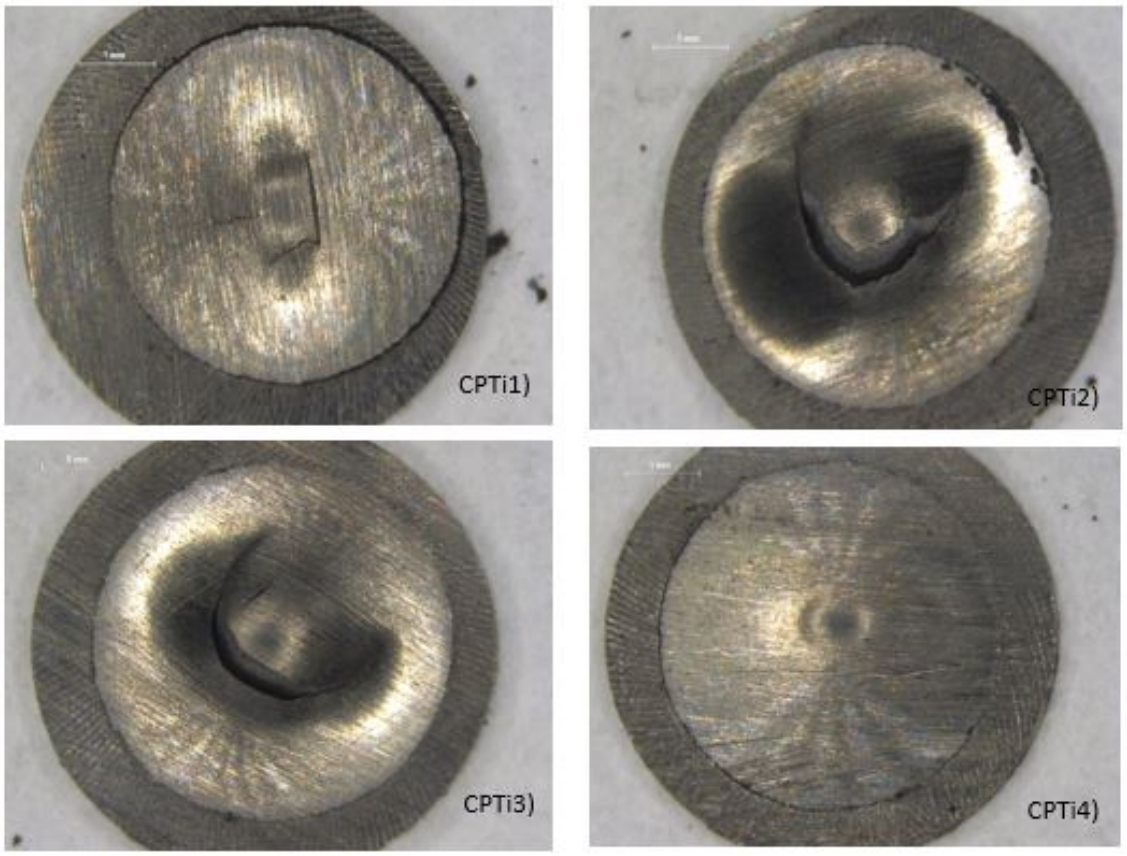

Figure 57: Optical Microscopy observation (magnitude 8 times) of the CPTi

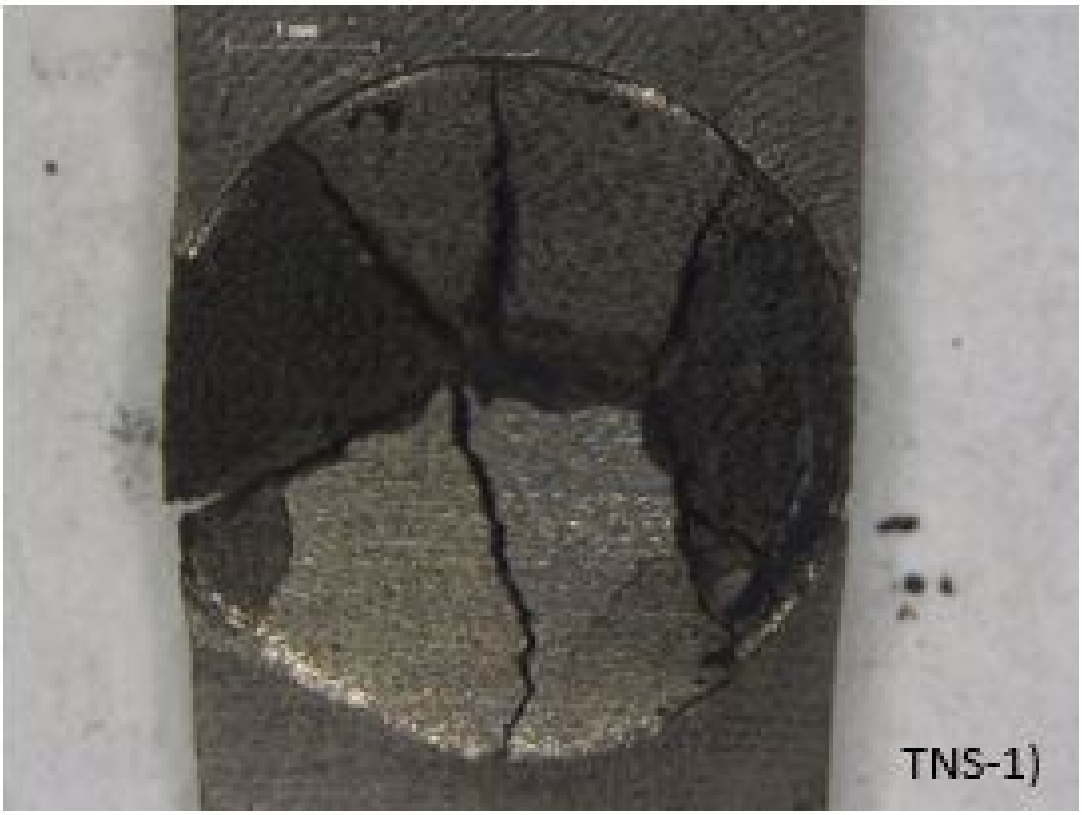

Figure 58: Optical Microscopy observation (magnitude 8 times) of the TNS-1

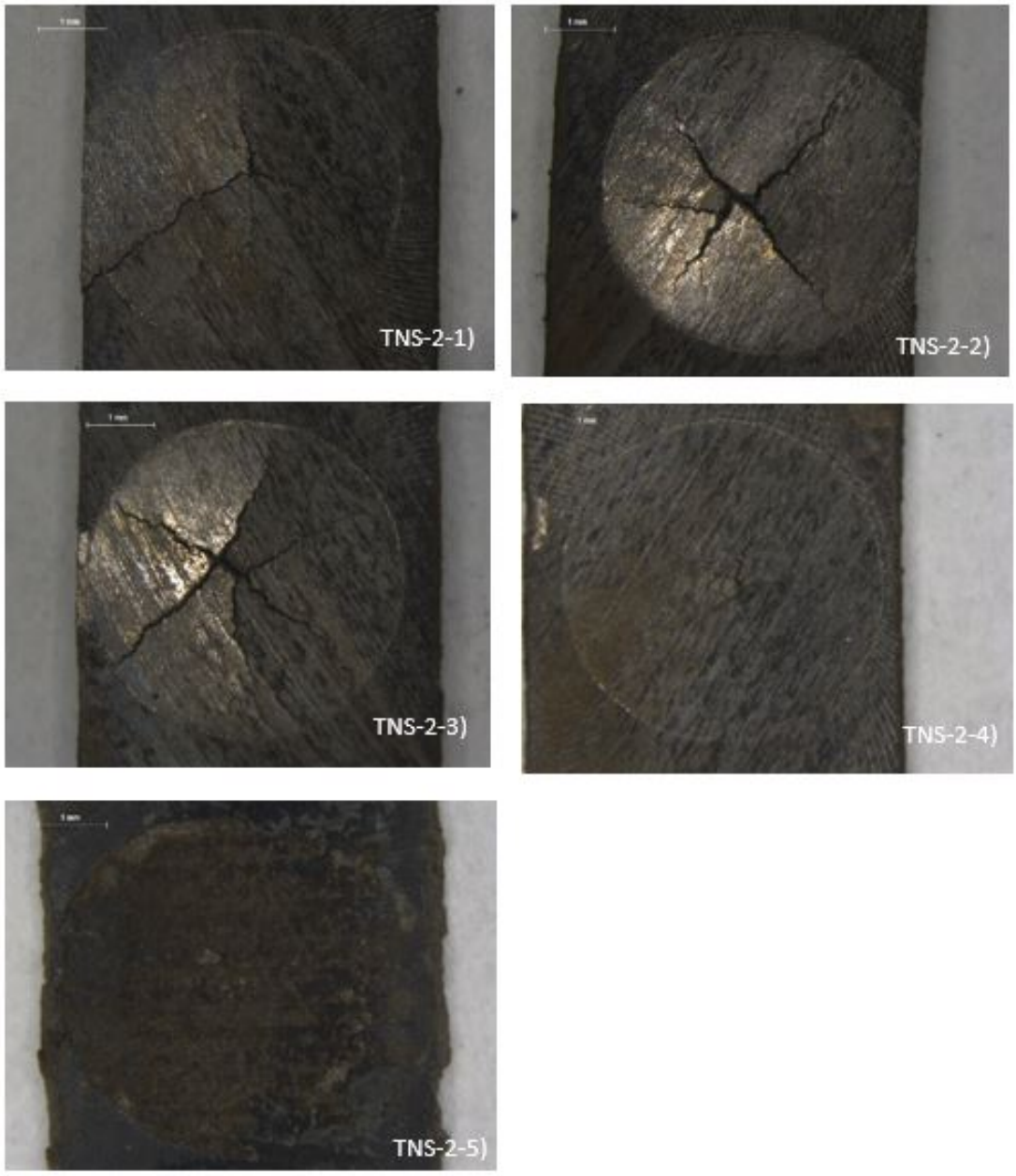

Figure 59: Optical Microscopy observation (magnitude 8 times) of the TNS-2

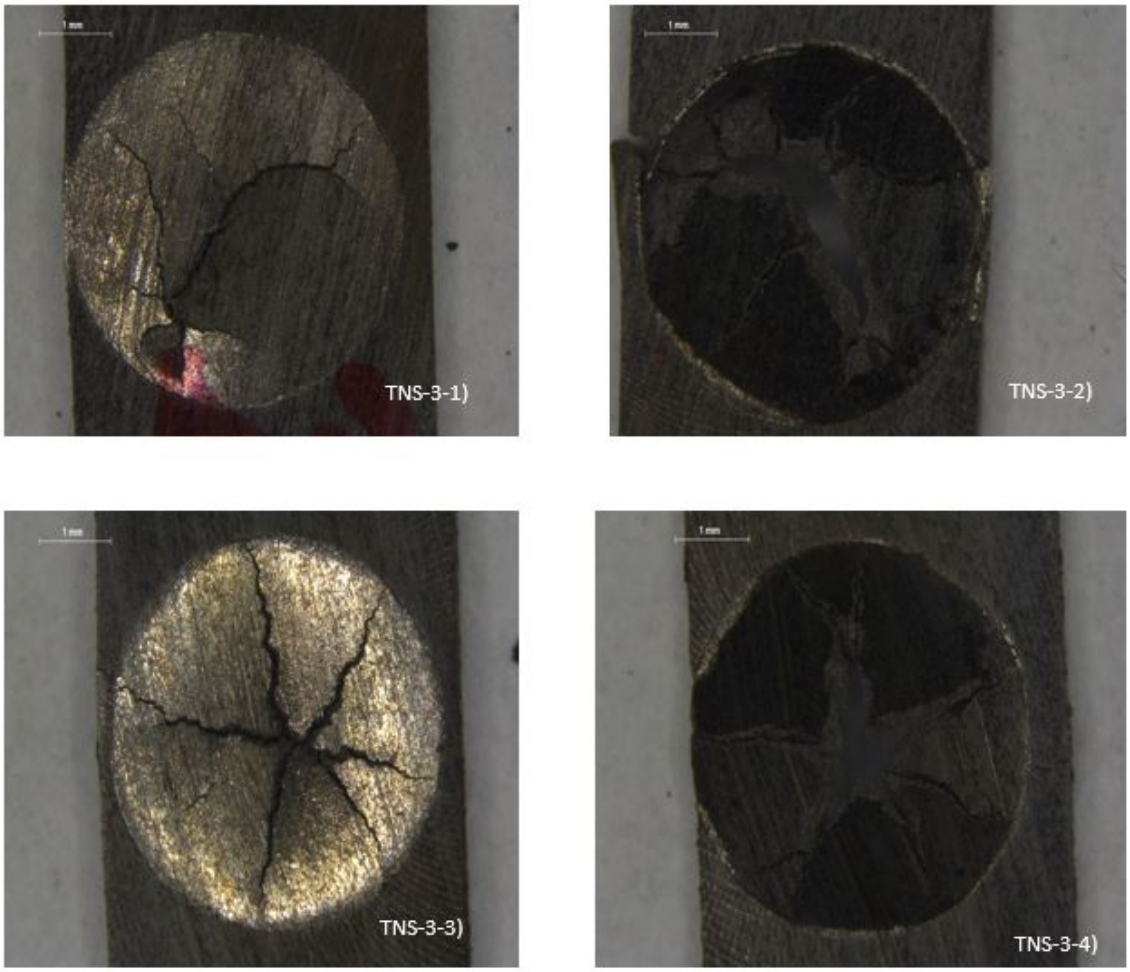

Figure 60: Optical Microscopy observation (magnitude 8 times) of the TNS-3

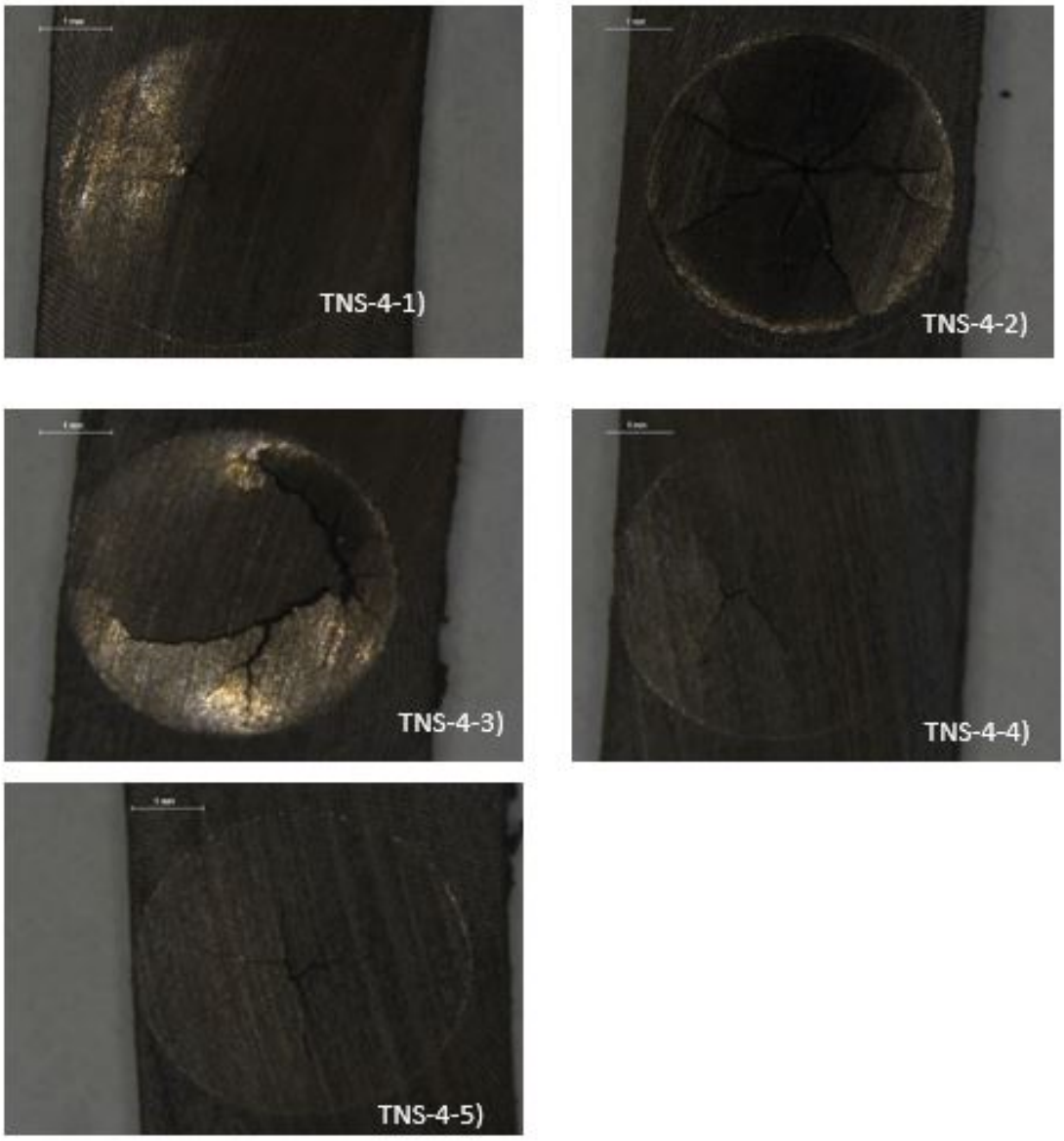

Figure 61: Optical Microscopy observation (magnitude 8 times) of the TNS-4

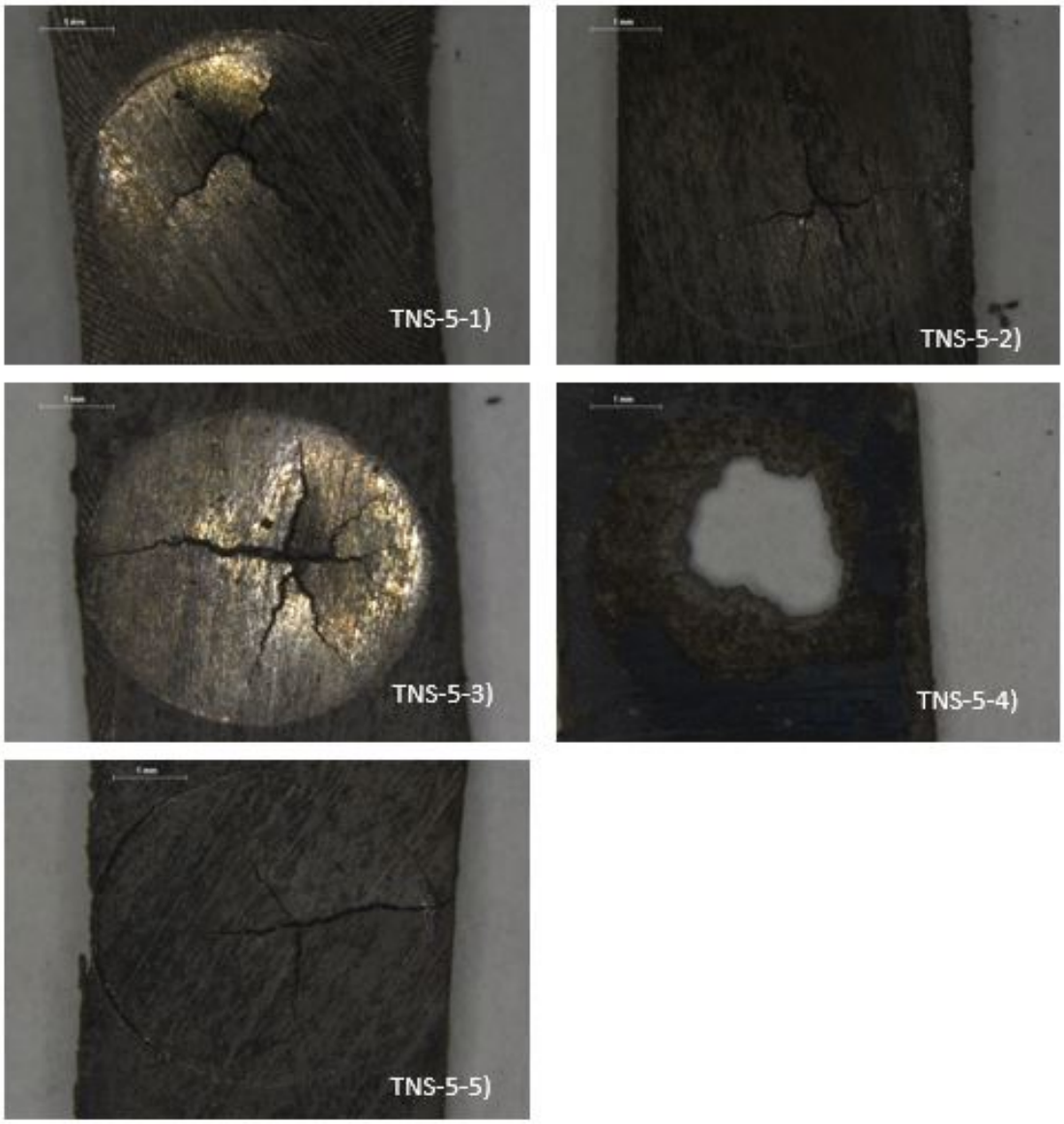

Figure 62: Optical Microscopy observation (magnitude 8 times) of the TNS-5

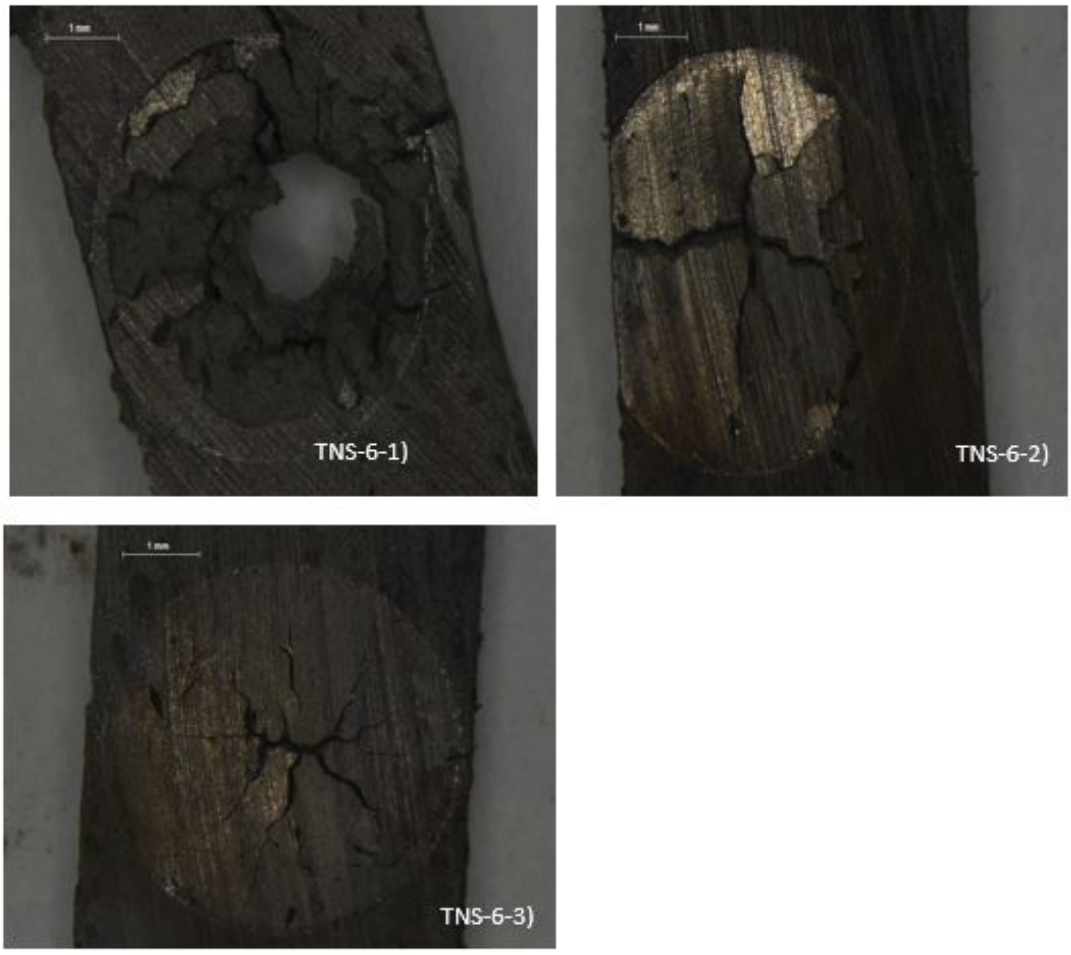

Figure 63: Optical Microscopy observation (magnitude 8 times) of the TNS-6

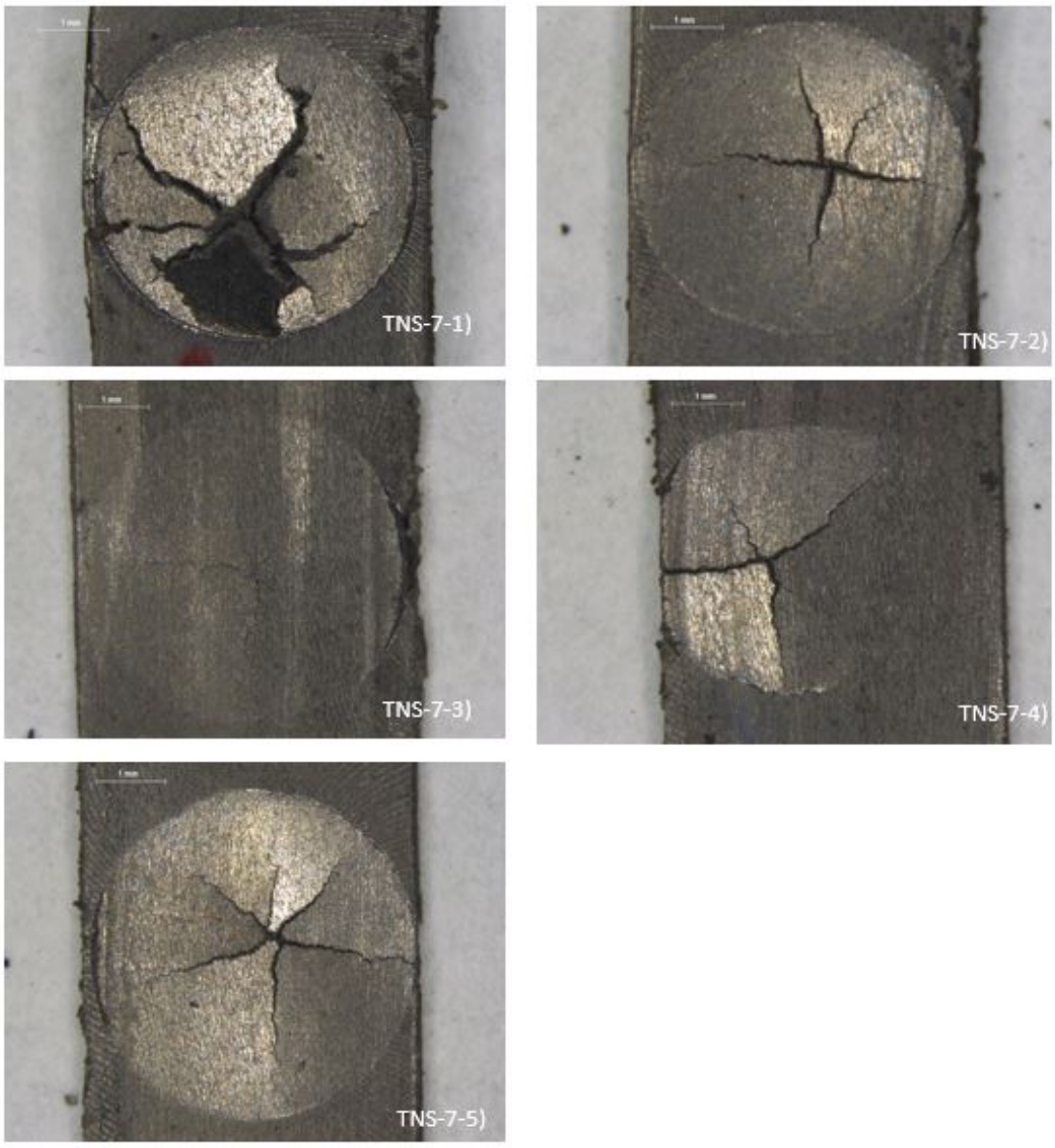

Figure 64: Optical Microscopy observation (magnitude 8 times) of the TNS-7

B.3 Results of Microtensile Test

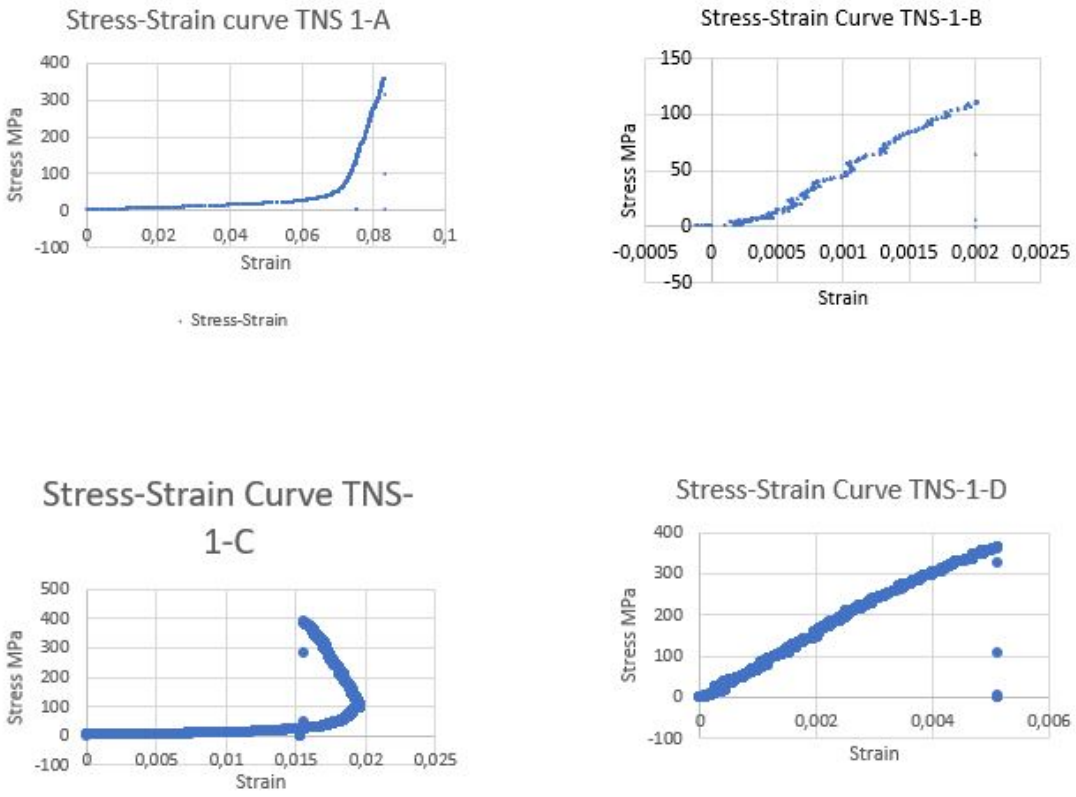

Figure 65: Stress - strain curve of the TNS-1 probe

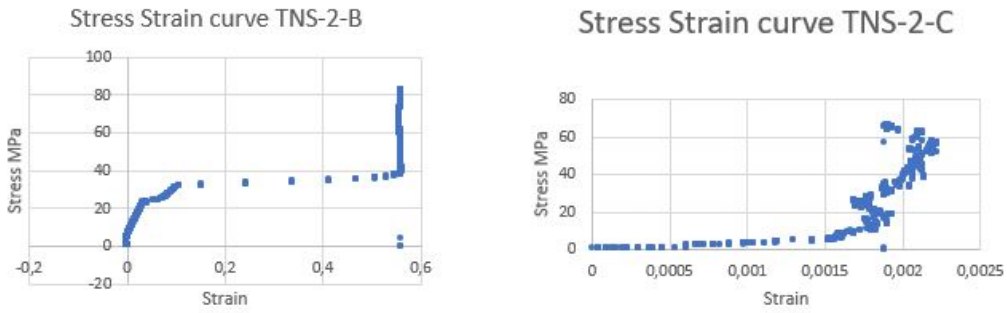

Figure 66: Stress - strain curve of the TNS-2 probe

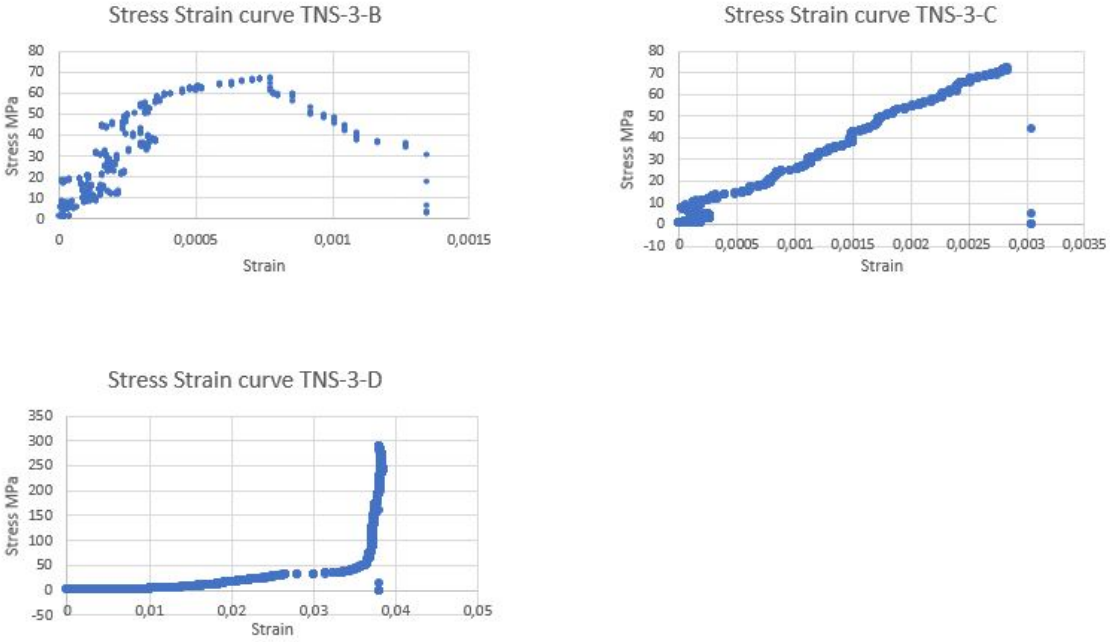

Figure 67: Stress - strain curve of the TNS-3 probe

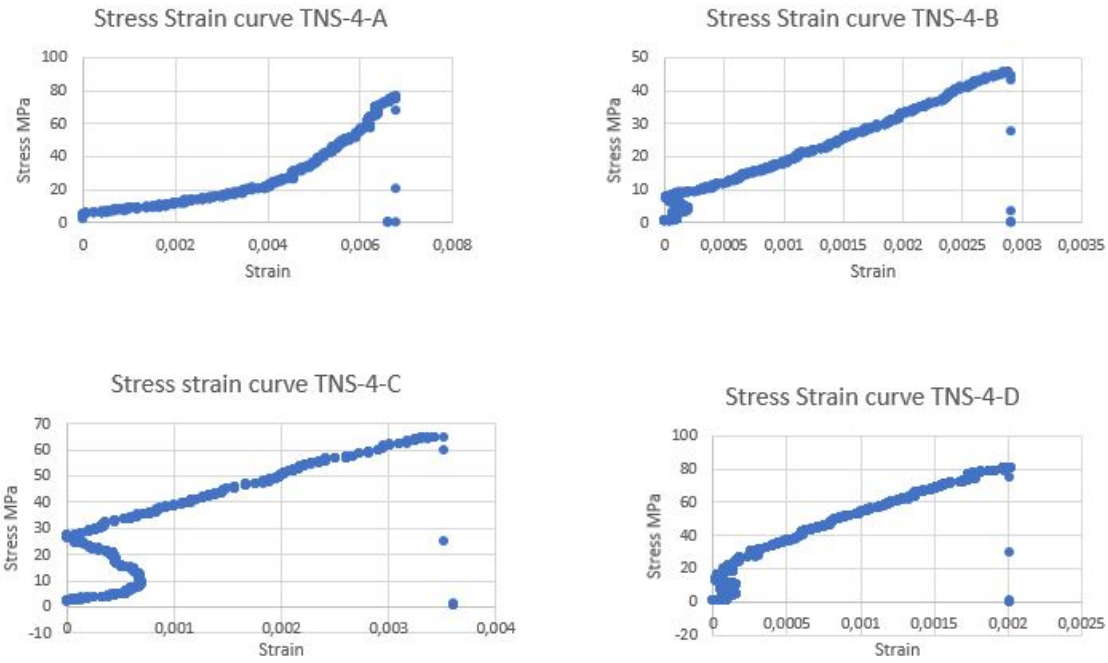

Figure 68: Stress - strain curve of the TNS-4 probe

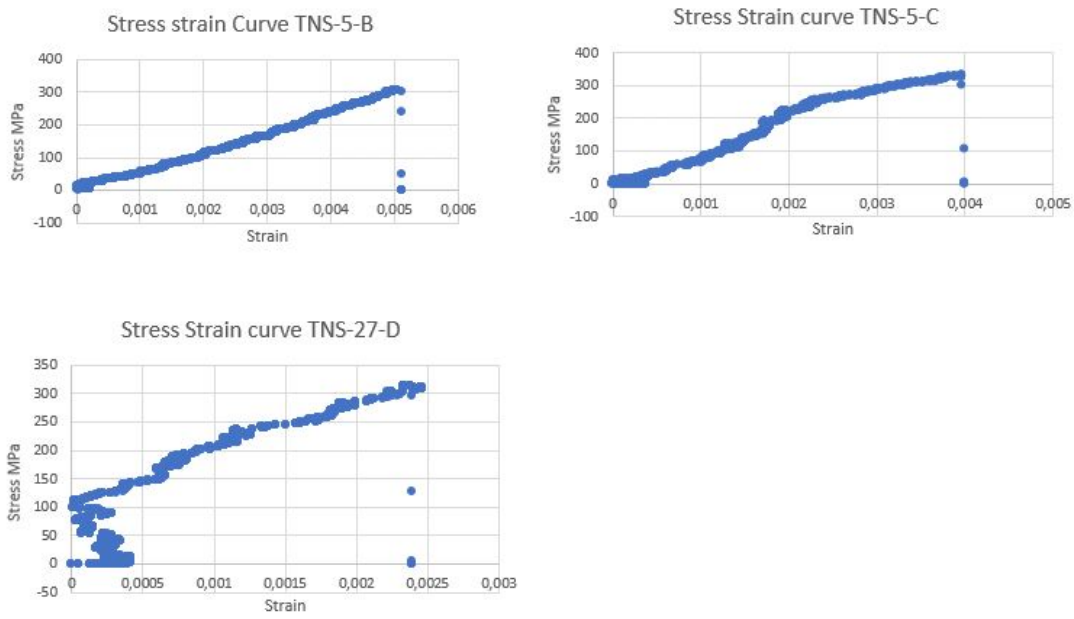

Figure 69: Stress - strain curve of the TNS-5 probe

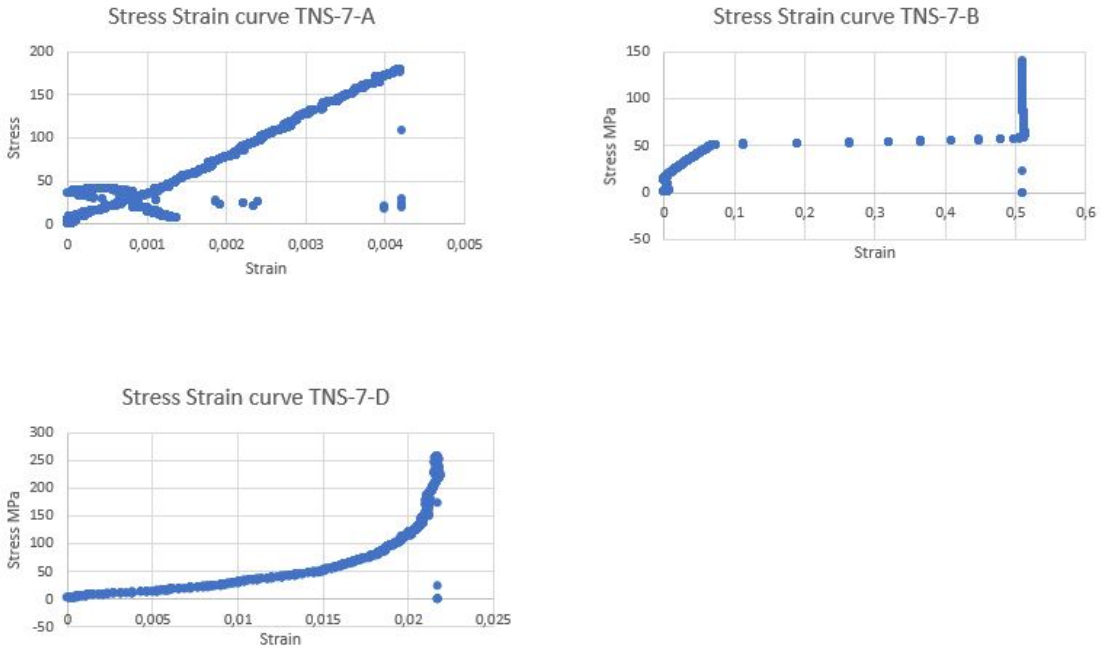

Figure 70: Stress - strain curve of the TNS-7 probe

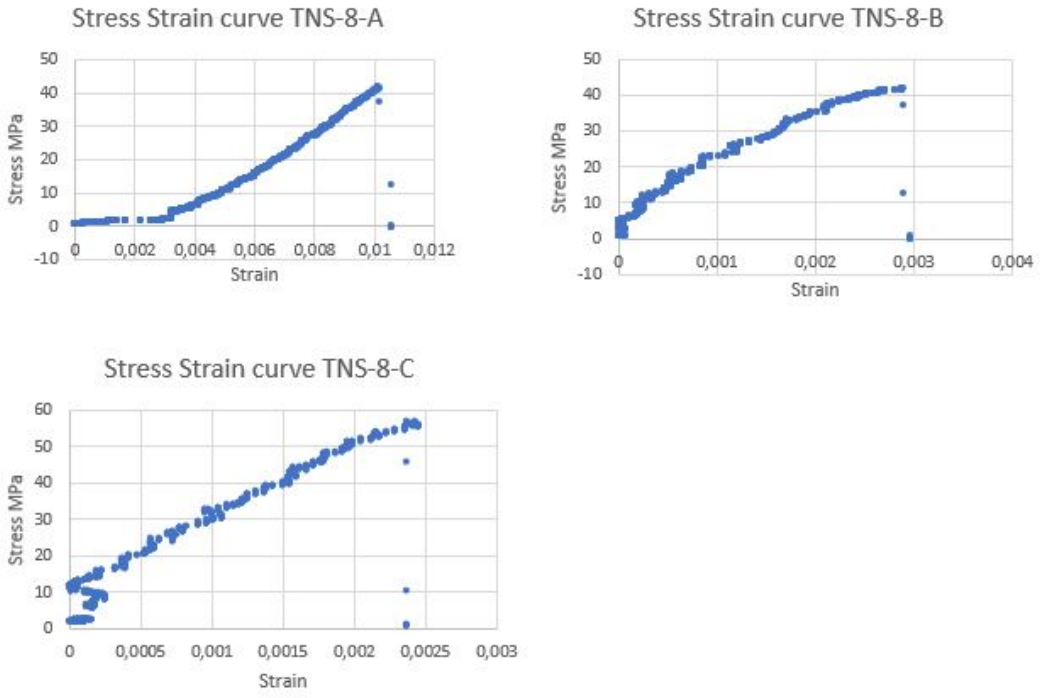

Figure 71: Stress - strain curve of the TNS-8 probe

Presupuesto del Trabajo Fin de Master: Validation of the mechanical properties of sintered material through the use of microprobes

Student: Nicolas Brunaut,
Tutor: Vicente Amigó Borrás

UNIVERSITAT POLITÈCNICA DE VALÈNCIA

January, 10, 2021

Contents

List of Tables

1 Introduction

This report is a part of the "Trabajo Fin de Master (**TFM**): Validation of the mechanical properties of sintered material through the use of microprobes".

The aim of this project is to have an overview of the budget of this TFM, and an idea of the necessary budget of a such work. This report will be divided into two main parts. The first one, the funding of the project and the second one, the budget of it. The budget will take into account the direct cost which means the cost of the workforce, the price of the materials, and machines used. The overhead costs (assumed equal at 10%) and the know-how tax (assumed equal at 10%) will be added at the end of the budget. In addition, the value added tax (**VTA**) will at the end added with a value of 21% to the all budget of the project.

2 Funding

This work has been funded by the Department of Mechanical and Material Engineering of the Technical and Higher Industrial School of Engineers at the *Universitat Politècnica de València*.

3 Budget

3.1 Direct cost

For the use of the machines, the amortization have been calculated from the equation 1 where t is the utilisation time of the machine during the project, C is the cost of the machine and T is the amortization period. T was considered equal to 10 years. Thanks to this equation, the machinery has been calculated as an unitary cost.

$$A = \frac{t * C}{T} \tag{1}$$

The price of the device was when it was possible the price of the exact device, material. Nevertheless if it was not possible to find it, it corresponds to an equivalent device or material.

3.1.1 Price of the workforce

Table 1: Table of the price of workforce

Units	Description	Unit Price (€)
h	Project Manager	25.00
h	Project co-director	25.00
h	Research	25.00
h	Chemical engineer	18.00
h	Mechanical engineer	18.00
h	Laboratory assistant	15.00

3.1.2 Price of the material

i Raw material and reagents

Table 2: Table of the price for raw material and reagents

Units	Description	Unit Price (€)
u	TiCP grade 3 bar	30
u	TNZT bar	60
g	Titanium Powder	0.018
g	Niobium Powder	0.15
g	Tin Powder	0.048
g	NaCl	$9.5 * 10^-5$
mL	Argon gaz	$2 * 10^-3$
mL	Solution for Ultrasound	$1.179 * 10^-2$
mL	Solution of ethanol and acetone	$8.679 * 10^-4$

ii Laboratory materials

Table 3: Table of the price for Laboratory Material

Units	Description	Unit Price (€)
u	Spoon	4.00
u	Beaker 100mL	1.80
u	Beaker 1L	9.04
u	P500 grinding paper	6.35
u	P100 grinding paper	25.00
u	Tweezers	1.80
u	450mL metallic jar	9.40
h	Diamond disk for slicer	588
h	MOD 13 disk	1.22
u	Cruciform	6.41

iii Personal Protective Equipment (PPE)

Table 4: Table of the price for Personal Protective Equipment

Units	Description	Unit Price (€)
u	Latex Gloves	0.052
u	Extinguisher	26.99
u	Bucket of sand	17.98

3.1.3 Price of the devices

Table 5: Table of the price for the devices

Units	Description	Unit Price (€)
u	Transparent Vacuum Glove boxe	17800
u	High precision scale	621.60
u	Planetary mill PM400/2 of Retsch	13195.00
u	Versina 2L of Bioengineering	3500
u	Furnace COMBUSTOL	28000.00
u	Acutom 10 of Struers	21787
u	Metallic saw	2.50
u	ELMASONIC S30H	678.00
u	Small Punch Test Machine	5128.00
u	Shimadzu Autograph X-Plus 100 Kn	5128.00
u	Optical Nikon-ECLIPSE LV100 DA-V	80000.00
u	Mitutoyo digimatic indicator ID-C150B	367.20
u	Electronic Digital Caliper 0-150 mm	178.00
u	BRUKER/2D Phaser	40000

3.2 Execution budget

Table 6: Executive budget for the fabrication of alloy through sintering process

Units	Description	Unit Price (€)	Quantity	Total (€)
u	**Fabrication alloy**			
h	Mechanical engineer	18.00	2.00	36.00
h	Laboratory assistant	15.00	2.00	30.00
g	Titanium Powder	0.018	93.5	1.683
g	Niobium Powder	0.15	52.983	7.95
g	Tin Powder	0.048	9.35	0.45
g	NaCl	$9.5 * 10^-5$	2.259	$2.14 * 10^-4$
mL	Argon gaz	$2 * 10^-3$	6300	12.6
u	Spoon	4.00	1.00	4.00
u	450mL metallic jar	9.40	2.00	18.8
h	Transparent Vacuum glove boxe	17800	1.00	0.20
h	High precision scale	621.60	1.00	$7.1 * 10^-3$
h	Planetary mill PM400/2 of Retsch	13195.00	72.00	10.85
h	Versina 2L of Bioengineering	3500	1.33	0.053
h	Furnace COMBUSTOL	28000	4.00	1.28
h	Bucket of sand	17.98	1.00	$2.05 * 10^-4$
u	Extinguisher	26.99	1.00	26.99
			Total price	150.86

Table 7: Executive budget for fabrication of sample of Small Punch Test

Units	Description	Unit Price (€)	Quantity	Total (€)
u	**Fabrication of sample of Small Punch Test**			
h	Mechanical engineer	18.00	0.25	4.50
h	Laboratory assistant	15.00	0.25	3.75
mL	Solution for Ultrasound	$1.179 * 10^{-}2$	10.00	1.179
mL	Solution of ethanol and acetone	$8679 * 10^{-}4$	10.00	$8.679 * 10^{-}2$
h	Beaker 100mL	1.80	0.2	$4.1 * 10^{-}6$
h	Beaker 1L	9.04	0.2	$2.06 * 10^{-}5$
10h	P500 grinding paper	6.35	1.00	0.635
10h	P100 grinding paper	25.00	1.00	2.50
1000h	Diamond disk for slicer	588	0.13	0.076
10h	MOD 13 disk	1.22	0.13	0.015
h	Cruciform	6.41	1.00	$7.32 * 10^{-}5$
h	Mitutoyo digimatic indicator ID-C150B	367.20	0.016	$6.70 * 10^{-}4$
h	Electronic Digital Caliper 0-150 mm	178.00	0.016	$3.25 * 10^{-}4$
u	Latex Gloves	0.052	2.00	0.104
h	Acutom 10 of Struers	21787	0.13	0.03
10h	Metallic saw	2.50	0.30	0.075
h	ELMASONIC S30H	678.00	0.30	$2.32 * 10^{-}3$
			Total price	12.95

Table 8: Executive budget for fabrication of sample of Microtension tensile test

Units	Description	Unit Price (€)	Quantity	Total (€)
u	**Fabrication of Microtension tensile test sample**			
h	Mechanical engineer	18.00	0.25	4.50
h	Laboratory assistant	15.00	0.25	3.75
mL	Solution for Ultrasound	$1.179 * 10^-2$	10.00	1.179
mL	Solution of ethanol and acetone	$8679 * 10^-4$	10.00	$8.679 * 10^-2$
h	Beaker 100mL	1.80	0.2	$4.1 * 10^-6$
h	Beaker 1L	9.04	0.2	$2.06 * 10^-5$
10h	P500 grinding paper	6.35	1.00	0.635
10h	P100 grinding paper	25.00	1.00	2.50
h	Diamond disk for slicer	588	0.13	0.076
10h	MOD 13 disk	1.22	0.13	0.015
h	Cruciform	6.41	1.00	$7.32 * 10^-5$
h	Mitutoyo digimatic indicator ID-C150B	367.20	0.016	$6.70 * 10^-4$
h	Electronic Digital Caliper 0-150 mm	178.00	0.016	$3.25 * 10^-4$
u	Latex Gloves	0.052	2.00	0.104
h	Acutom 10 of Struers	21787	0.13	0.03
10h	Metallic saw	2.50	0.30	0.075
h	ELMASONIC S30H	678.00	0.30	$2.32 * 10^-3$
			Total price	12.95

Table 9: Executive budget for the Small Punch Test

Units	Description	Unit Price (€)	Quantity	Total (€)
u	**Small Punch Test**			
h	Mechanical engineer	18.00	0.08	1.44
h	Laboratory assistant	15.00	0.08	1.2
u	Tweezers	1.80	2.00	3.60
h	Cruciform	6.41	1.00	$7.32 * 10^-5$
h	Small Punch Test Machine	5128.00	0.08	$4.68 * 10^-3$
			Total price	6.24

Table 10: Executive budget for the Microtension Test

Units	Description	Unit Price (€)	Quantity	Total (€)
u	**Microtension Test**			
h	Mechanical engineer	18.00	0.08	1.44
h	Laboratory assistant	15.00	0.08	1.2
h	Electronic Digital Caliper 0-150 mm	178.00	0.016	$3.25 * 10^-5$
h	Shimadzu Autograph X-Plus 100 Kn	5128.00	0.08	$4.68 * 10^-3$
			Total price	2.65

Table 11: Executive budget for the XRD Analysis

Units	Description	Unit Price (€)	Quantity	Total (€)
u	**Energy Dispersive X-ray Spectroscopy**			
h	Chemical engineer	18.00	0.15	2.7
h	Laboratory assistant	15.00	0.15	2.25
h	XRD machine	40000	24.000	10.96
			Total price	15.9

Table 12: Executive budget for Small Punch Test analysis

Units	Description	Unit Price (€)	Quantity	Total (€)
u	**Small Punch Test analysis**			
h	Mechanical engineer	18.00	0.05	2.7
h	1years Excel licence	135.00	0.05	$7.7 * 10^-4$
h	1years Origin licence	350.00	0.05	$2.00 * 10^-3$
			Total price	2.7

Table 13: Executive budget for Microtension Test analysis

Units	Description	Unit Price (€)	Quantity	Total (€)
u	**Microtension Test analysis**			
h	Mechanical engineer	18.00	0.05	2.7
h	1years Excel licence	135.00	0.05	$7.7 * 10^-4$
h	1years Origin licence	350.00	0.05	$2.00 * 10^-3$
			Total price	2.7

3.3 Overall Budget

Table 14: Executive budget for the research

Description	Price (€)	Quantity	Total (€)
u	**Executive budget research**		
Fabrication of alloy through sintering process	150.86	8	1206.88
Fabrication of sample of Small Punch Test	12.95	37	479.15
Fabrication of sample of Microtension Test	12.95	28	362.6
Small Punch Test	6.24	37	230.88
Microtension Test	2.65	28	74.2
XRD Analysis	15.9	9	143.1
Small Punch Test analysis	2.7	37	99.9
Microtension Test analysis	2.7	28	75.6
		Total price without taxes	2672.31
		10% Overhead costs	267.23
		10% Know-how	267.23
		21% V.A.T.	561.12
		Investment Budget	3767.89

The overall budget of this research is THREE THOUSAND SIXTY-SEVEN EUROS AND EIGHTY-NINE CENTS.